JOURNAL OF GEOPHYSICAL RESEARCH, VOL. 92, NO. C2, PAGES 1507–1526, FEBRUARY 15, 1987

Seasonal Cycles of Currents, Temperatures, Winds, and Sea Level Over the Northeast Pacific Continental Shelf: 35°N to 48°N

P. T. STRUB, J. S. ALLEN, A. HUYER, AND R. L. SMITH

College of Oceanography, Oregon State University, Corvallis

R. C. BEARDSLEY

Woods Hole Oceanographic Institution, Woods Hole, Massachusetts

Seasonal cycles of coastal wind stress, adjusted sea level (ASL), shelf currents, and water temperatures off the west coast of North America (35°N to 48°N) are estimated by fitting annual and semiannual harmonics to data from 1981–1983. Longer records (9–34 years) of monthly ASL indicate that these two harmonics adequately represent the long-term monthly average seasonal cycle and that the current measurement period is long enough to estimate the seasonal cycles. We characterize the differences between fall/winter and spring/summer as follows: For fall/winter, monthly mean winds north of 35°N are northward for 3–6 months (longer in the north than in the south); south of 35°N, the mean winds are near zero or weakly southward; monthly mean alongshore currents are northward over midshelf and shelf break at all locations sampled at depths of 35 m and deeper and are associated with high coastal sea levels and relatively warm water temperatures. For spring/summer, monthly mean wind stresses are southward at all latitudes for 3–6 months (longer in the south than in the north), sea levels are low, and water temperatures are relatively cool; monthly mean currents at 35 m depth over the shelf are southward for 1–6 months (longer at the shelf break than over midshelf and longer in the north than in the south), while the deeper currents are less southward or northward. The magnitudes of the seasonal cycles of all variables are maximum between approximately 38°N and 43°N, generally decreasing slightly to the north and greatly to the south. At each location the seasonal cycle of the alongshore current from 35 m depth at midshelf leads the sea level slightly and both lead the wind stress and temperatures by 1–2 months. The seasonal cycles of all variables show a south-to-north progression (south leads north by 1–2 months). At 48°N, annual mean currents at 50 m depth over the shelf break oppose the annual mean wind (northward wind and southward current). Similarly, at 35°N, annual mean currents at 35 m depth over both midshelf and shelf break are opposed to the annual mean wind (southward wind and northward current). From 35°N to 43°N, both summer and winter regimes are dominated by strongly fluctuating currents.

INTRODUCTION AND BACKGROUND

Over the past 20 years a conceptual picture of the coastal current system off the west coast of North America has developed, largely on the basis of current and hydrographic measurements made off Oregon, Washington, and British Columbia [*Huyer et al.*, 1975, 1978, 1979; *Hickey*, 1979; *Freeland et al.*, 1984] and hydrographic data collected off southern California [*Chelton*, 1984]. In its simplest form this conceptual picture consists of two regimes: a fall and winter regime, characterized by alongshore currents which are northward and barotropic in the mean, with large, low-frequency baroclinic fluctuations, and a spring and summer regime, characterized by baroclinic, persistently southward surface currents over a northward undercurrent, with barotropic low-frequency fluctuations. The current measurements used to develop this picture were usually of short duration and irregularly sampled in space, raising questions of how well this picture represents the large-scale structure of the coastal currents and whether or not the timing of the seasonal cycle of currents at a given location is determined by local wind-forcing alone. The seasonal cycle of wind stress is strongest between 39°N and 42°N, south of most historical current measurements, raising the question of whether the seasonal cycle of currents is stronger and more regular (accounting for more of the variance) at those latitudes, with a decrease in magnitude both to the north and the south.

In this paper we explore the structure and timing of the seasonal cycles of currents and temperatures in the coastal ocean, using current measurements from moorings maintained as part of several experiments at midshelf and shelf break locations off the west coast of North America (approximately 35°N to 48°N), from spring 1981 to fall 1982. We also discuss the seasonal cycles of sea level and wind stress using data from the same period. Sea level data from longer periods are used to determine whether or not the period of the mooring data allows an adequate determination of the seasonal cycles.

Several aspects of the seasonal cycle can be discussed. First, the seasonal cycles of wind stress, sea level, current, and temperature can be described, and the relative magnitudes and phases of these cycles at different locations can be compared. It is this aspect that is emphasized in this paper. Another aspect involves the seasonal variation of fluctuations with periods of a day to a month. While seasonal variations in these short-term fluctuations can be seen in the data and are discussed qualitatively, a detailed analysis of these fluctuations is not presented here. A final aspect of the seasonal cycle concerns the amount of variability in the cycles from year to year. Except for the sea level records the present data set is too short to quantify interannual differ-

Paper number 6C0437.
0148-0227/87/006C-0437$05.00

TABLE 1. Location, Depths, Periods, and Statistics of Low-Passed Current and Temperature Time Series

Location		Total Mooring Period	Identification	Water Depth, m	Nominal Sensor Depth, m	Average			Orientation of Principal Axis, °T	Standard Deviation		
Latitude	Longitude					$\bar{u}$, cm/s	$\bar{v}$, cm/s	$\bar{T}$, °C		Major, cm/s	Minor, cm/s	T, °C
Barkley Sound, British Columbia, 48.3°N, 125.8°W		Feb. 1981 to July 1982	Z3S1	210	50	3.3	−0.5	9.04	314	14.4	5.4	0.74
			Z3S2	210	100	0.4	0.8	7.94	314	10.9	3.3	0.56
			Z3S3	210	150	−4.3	1.1	7.27	286	8.7	2.6	0.40
Coos Bay, Oreg., 43.1°N, 124.6°W		April 1981 to Nov. 1983	Q3S1	97	35	0.4	1.7	9.74	8	16.8	4.2	1.54
			Q3S2	97	65	−0.3	4.4	8.98	2	12.7	3.3	1.45
			Q4S1	133	35	−0.3	−3.0	9.93	16	21.3	6.9	1.32
			Q4S2	133	65	0.4	1.6	9.20	10	18.5	5.5	1.36
			Q4S3	133	105	−0.3	5.4	8.34	349	12.6	2.6	1.05
CODE, California, 38.6°N, 123.5°W		April 1981 to Nov. 1982	C3S1	90	35	−0.2	1.8	10.19	323	19.2	4.2	1.43
			C3S3	90	65	−3.6	3.0	9.41	323	11.4	4.1	1.04
San Francisco, Calif., 37.4°N, 122.9°W		April 1981 to Aug. 1982	H3S1	83	35	4.7	2.2	10.93	341	7.5	4.2	1.16
			H3S2	83	65	−0.6	2.1	10.04	330	4.7	2.5	0.92
Purisima Point, Calif., 34.7°N, 120.8°W		Feb. 1981 to Aug. 1982	P3S1	95	35	3.5	3.4	11.86	2	11.4	5.1	0.67
			P3S2	95	65	0.8	4.5	10.82	356	7.9	3.5	0.58
			P4S1	155	35	−2.1	6.1	11.82	358	13.6	5.4	0.55
			P4S2	155	65	−0.2	8.2	10.65	346	11.4	4.1	0.47
			P4S3	155	125	−0.2	6.6	9.65	348	7.2	2.0	0.29

The average current is given in terms of eastward (u) and northward (v) components; the standard deviations are given for components along the principal axes. These statistics are calculated for a 1-year period from May 1, 1981, to May 1, 1982.

ences but does provide a basis for comparison with past and future records, contributing to the eventual quantification of both the true long-term annual cycles and their interannual variability. The data from the midshelf mooring at 43°N does show the effects of the 1982–1983 El Niño, as is discussed in detail by *Huyer and Smith* [1985]; the sea level data allows an extension of their results to the entire coastal ocean from 33°N to 48°N.

Data and Methods

Table 1 presents the locations of the moorings, nominal depths of the sensors, the approximate period of available data, and statistics of the data. The bathymetry around the mooring locations can be seen in Figure 1. These data come from three different projects. Data from the midshelf mooring at 38.6°N were collected as part of the Coastal Ocean Dynamics Experiment (CODE) [*Coastal Ocean Dynamics Experiment Group,* 1983], as is described by *Beardsley and Rosenfeld* [1983] and *Beardsley et al.* [1985a]. Data from the shelf break mooring at 48.3°N (on a line off Carmanah Point near Barkley Sound) were part of a Canadian study of the currents off Vancouver Island, described by *Freeland et al.* [1984] and *Thomson et al.* [1985]. This mooring was in 210 m of water, with instruments at depths of approximately 50 m, 100 m, and 150 m. The other moorings were in an array designed to provide the large-scale picture from 35°N to 43°N, as part of a project called SuperCODE. In the SuperCODE array, current meters on taut subsurface moorings were used to measure currents and temperatures at 35 m and 65 m depths at midshelf (approximately the 90-m isobath) and over the shelf break (approximately the 150-m isobath), with additional measurements at 125 m over the shelf break. All moorings were replaced at intervals of 3 to 6 months. Further details of the SuperCODE moored data collection and reduction can be found in the work by *Denbo et al.* [1984]. Moorings were successfully maintained at both midshelf and shelf break locations at two latitudes: 34.7°N (Purisima Point) and 43.1°N (Coos Bay). At 37.4°N (San Francisco), only the midshelf mooring was successfully maintained over the entire period. The actual depths of the individual mooring deployments and sensor depths varied slightly from mooring to mooring, but no attempt has been made to adjust the data to compensate for the changes in sensor depth. Over a year of current and temperature data from midshelf and shelf break mooring sites are available at 34.7°N and 43.1°N, and data from single mooring sites are available from 37.4°N, 38.6°N, and 48.3°N. The midshelf moorings are Q3, C3, H3, and P3; the shelf break moorings are Z3, Q4, and P4 (Table 1). The midshelf mooring at 43.1°N was maintained through the end of 1983, providing nearly 3 years of data.

In addition to the data from the moorings, wind stress and sea level data were collected, as is described by *Halliwell and Allen* [1983]. The wind velocities are either hourly measurements from near-shore buoys and onshore coastal sites or velocities calculated from 6-hourly Fleet Numerical Oceanographic Center synoptic surface pressure fields, arrayed on a 3° grid [*Bakun,* 1973, 1975]. These "calculated" winds are geostrophic winds computed from surface pressure fields, then reduced by 30% and rotated 15° to the left to approximate surface frictional effects. Stresses derived from measured winds are referred to as "measured" wind stresses, while those derived from the "calculated winds" are called calculated wind stresses. For consistency, all wind stresses were computed from wind velocities using the bulk formula of *Large and Pond* [1981], though this formula was originally intended for use with only overwater wind velocities. Locations and periods of both kinds of wind stress data are given in Table 2. Measured winds were collected at other stations as well, but orographic problems and data gaps were judged to be least for the locations presented here. Eight coastal locations are shown, consisting of four shore stations, three National Data Buoy Office (NDBO) buoys from over the shelf, and one island. Data from two buoys farther offshore are also presented. The buoy winds are presumably free of local topographic interference but suffer from data gaps, especially in the winter. Calculated wind stresses from nine latitudes have been used, from 26.0°N to 48.2°N. Since

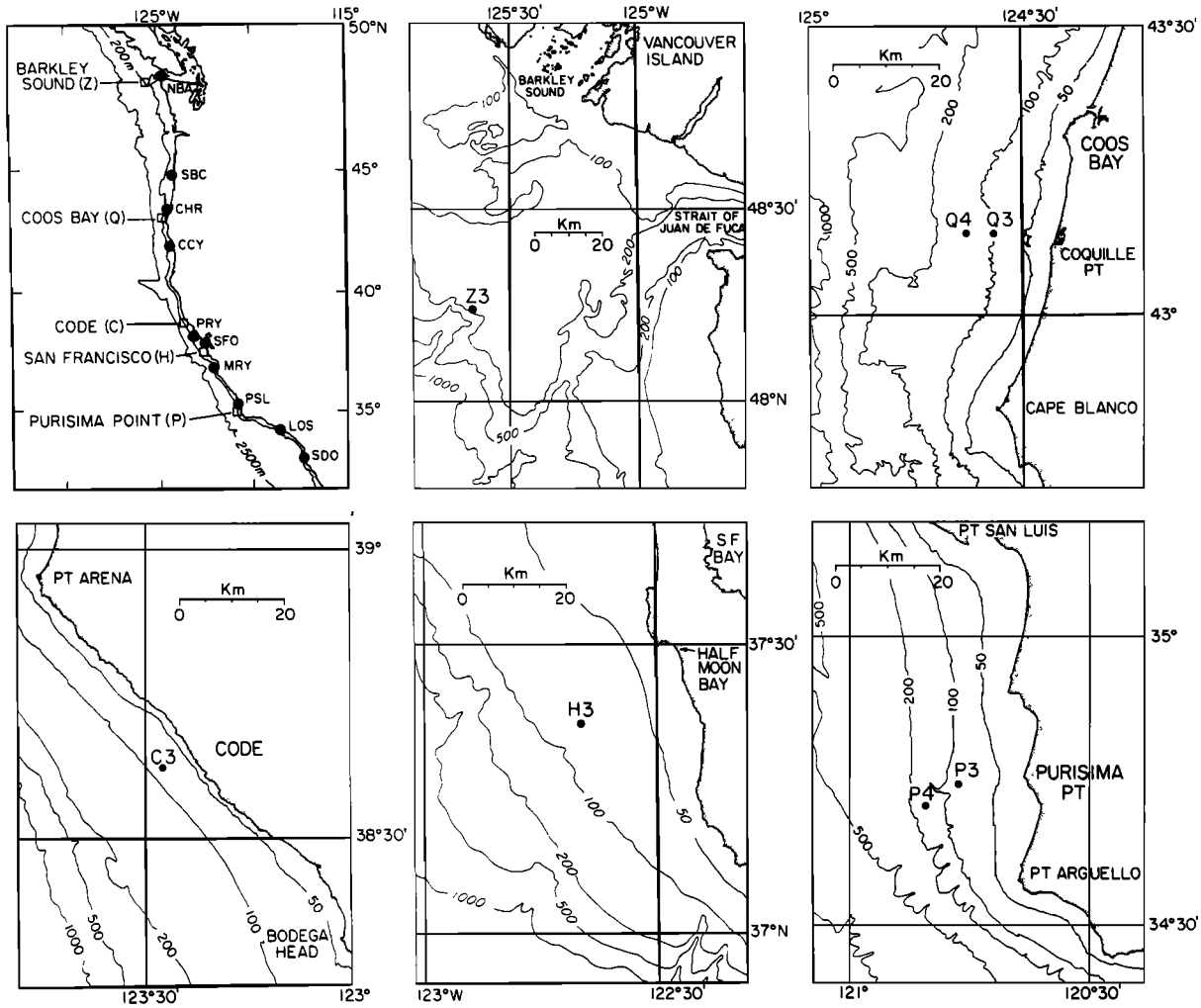

Fig. 1. The locations of the five mooring sites (open squares) and sea level data (solid circles) are shown at the top left. Details of the bathymetry around each mooring are shown in the other panels (isobath depths are in meters). Note the change in horizontal scale of the map for Z3 (48°N).

these winds are calculated from smoothed 6-hourly pressure fields on a 3° grid, they have less energy at the shorter space and time scales than the measured winds and are more coherent over large space scales. Their advantage is their lack of data gaps and their availability at all times and locations. A combination of nine full years of calculated wind data were available for analysis, 1971 through 1975 and 1980 through 1983.

Locations, periods, and statistics of the sea level data are given in Table 3. At some of the 10 locations the periods for the hourly data are the same 9 years as for the calculated wind stress. At other locations, data are only available for the 1980–1983 period. Longer records (9–34 years) of monthly data are available at nine locations. All of the sea level data were adjusted by adding raw sea level (in centimeters) to atmospheric pressure ($p - 1000$ in millibars). The result is called adjusted sea level (ASL) and represents the total subsurface pressure that is important in the dynamics of the coastal ocean. The longer records of monthly ASL were first demeaned and detrended, and the hourly data were then demeaned and detrended using the trends found from the monthly data (the data from Los Angeles were only demeaned, since a long-term trend was not available from that location). The hourly data were filtered with a low-pass filter (LLP has a 46-hour half-power point) to remove tides, inertial, and diurnal signals, and decimated to 6-hourly values. For purposes of display only (Figures 4, 5, 10, 11, and 12), the data were further low pass–filtered (LP5 has a half-power point of 5 days) before plotting. The monthly means were also used to calculate more representative, long-term annual cycles of ASL for comparison with the annual cycles determined from the shorter mooring periods.

The usual method of calculating the seasonal cycle of a multiyear time series is to calculate the long-term average for each calendar month over the entire series. We refer to such seasonal cycles as the average monthly cycles. The 6-hourly time series of current, temperature, wind stress, and ASL in this study are too short to provide average monthly cycles. An alternative method to determine the seasonal cycle is to fit the data to annual harmonics (sine and cosine functions with periods of $1/n$ years, $n = 1, 2, \cdots$); this method is preferable for time series which are short or irregularly sampled in time [*Lynn*, 1967; *Chelton*, 1984; *Godfrey and Ridgway*, 1985]. The fit is usually limited to the first two harmonics ($n = 1, 2$) to avoid including higher-frequency features that may exist in the short data records but are not

TABLE 2. Locations, Periods, and Statistics of the Wind Stress

Identification	Approximate Location	Latitude, °N	Longitude, °W	Data Period	Average $\bar{\tau}_x$, dyn/cm²	Average $\bar{\tau}_y$, dyn/cm²	Orientation of Principal Axis, °T	Standard Deviation Major, dyn/cm²	Standard Deviation Minor, dyn/cm²
				Calculated (Bakun) Wind Stress					
CG13	Neah Bay, Wash.	48.2	124.7	Jan. 1971 to Dec. 1975 Jan. 1980 to Dec. 1983	0.108	0.428	343.7	1.516	0.854
CG10	Charleston, Oreg.	43.4	124.3	Jan. 1971 to Dec. 1975 Jan. 1980 to Dec. 1983	0.152	0.093	17.3	1.496	0.757
CG08	Humbolt, Calif.	40.2	124.3	Jan. 1971 to Dec. 1975 Jan. 1980 to Dec. 1983	0.145	−0.320	12.3	1.524	0.554
CG07	CODE site	38.7	123.5	Jan. 1971 to Dec. 1975 Jan. 1980 to Dec. 1983	0.183	−0.431	3.0	1.204	0.470
CG06	San Francisco, Calif.	37.3	122.4	Jan. 1971 to Dec. 1975 Jan. 1980 to Dec. 1983	0.252	−0.451	350.0	0.924	0.456
CG04	Purisima Point, Calif.	34.6	120.7	Jan. 1971 to Dec. 1975 Jan. 1980 to Dec. 1983	0.351	−0.523	331.7	0.742	0.465
CG01	Baja California	31.5	116.7	Jan. 1971 to Dec. 1975 Jan. 1980 to Dec. 1983	0.464	−0.709	313.2	0.776	0.295
CG34	Baja California	28.8	114.7	Jan. 1971 to Dec. 1975 Jan. 1980 to Dec. 1983	0.450	−0.431	300.6	0.517	0.250
CG32	Baja California	26.1	112.7	Jan. 1971 to Dec. 1975 Jan. 1980 to Dec. 1983	0.253	−0.294	303.7	0.341	0.233
				Measured Wind Stress					
CPD	Cape Disappointment, Wash.	46.3	124.1	Dec. 1980 to Nov. 1982	−0.029	0.486	351.7	1.178	0.647
SIU	Siuslaw River, Oreg.	44.0	124.1	Dec. 1980 to Nov. 1982	0.042	0.105	3.3	1.074	0.455
HUM	Humbolt Bay, Calif.	40.8	124.2	Dec. 1980 to Nov. 1982	0.005	−0.030	345.9	0.588	0.188
B14	NDBO buoy 46014	39.2	124.0	April 1981 to Nov. 1983	0.249	−0.296	335.4	1.171	0.285
B12	NDBO buoy 46012	37.4	122.7	Dec. 1980 to Nov. 1983	0.179	−0.172	332.3	0.712	0.242
SUR	Point Sur, Calif.	36.3	121.9	Dec. 1980 to Nov. 1982	0.127	−0.305	333.4	0.596	0.101
B11	NDBO buoy 46011	34.9	120.9	Dec. 1980 to Nov. 1983	0.299	−0.378	324.2	0.509	0.165
SNI	San Nicholas Island, Calif.	33.3	119.5	Dec. 1980 to July 1983	0.278	−0.248	314.1	0.490	0.109
B05	NDBO buoy 46005	46.0	131.0	Dec. 1981 to Nov. 1983	0.509	0.083	349.8	1.088	0.857
B02	NDBO buoy 46002	42.5	130.0	Dec. 1981 to Nov. 1983	0.290	−0.082	353.5	0.903	0.669

The average wind stress is given in terms of eastward (τ_x) and northward (τ_y) components; the standard deviations are given for components along the principal axes.

characteristic of the true seasonal cycles. The seasonal cycle of any variable is then

$$A(t) = A_0 + A_1 \cos(\omega t - \phi_1) + A_2 \cos(2\omega t - \phi_2) \quad (1)$$

where $\omega = 2\pi/(365.25 \text{ days})$, A_0 is the annual mean value, A_1 and A_2 are the magnitudes of the annual and semiannual harmonics, and ϕ_1 and ϕ_2 are the phases corresponding to the maxima in the cycles. The annual harmonic was always included, but the semiannual harmonic was only included if the fit was significant at the 80% confidence level. Details of the fitting procedure and tests of significance of the fit are found in the Appendix. Both the average monthly cycles and the harmonic fits were determined for the longer monthly ASL time series.

For the vector variables, principal axes were calculated, and the vectors were projected onto their major and minor axes. In general, the major axis components of the currents follow the local isobaths, and the major axis components of wind stresses follow the coastline. We use the term "alongshore components" to refer to the major axis components of both wind stresses and currents, while the minor axis components are called the "cross-shelf components." *Hal-*

TABLE 3. Locations, Periods, and Standard Deviations of Adjusted Sea Level

Identification	Location	Latitude, °N	Data Period Hourly Data	Data Period Monthly Data	Standard Deviation, cm January 1980 to December 1983	Standard Deviation, cm May 1981 to April 1982
NBA	Neah Bay, Wash.	48.4	1971–1975, 1980–1983	1950–1983	14.3	13.4
SBC	South Beach, Oreg.	44.6	1971–1975, 1980–1983	1967–1983	14.4	13.3
CHR	Charleston, Oreg.	43.3	1980–1983	1970–1983	13.1	12.0
CCY	Crescent City, Calif.	41.8	1971–1975, 1980–1983	1950–1983	12.4	10.7
PRY	Point Reyes, Calif.	38.0	1980–1983	1975–1983	10.6	8.0
SFO	San Francisco, Calif.	37.8	1971–1975, 1980–1983	1950–1983	10.5	7.3
MRY	Monterey, Calif.	36.6	1973–1975, 1980–1983	1964–1983	8.7	5.0
PSL	Port San Luis, Calif.	35.2	1980–1983	1950–1983	8.2	4.3
LOS	Los Angeles, Calif.	33.7	1971–1975, 1981–1983		8.0	4.0
SDO	San Diego, Calif.	32.8	1980–1983	1950–1983	8.2	4.1

liwell and Allen [1984, this issue] present a comparison of the principal axes of the measured and calculated wind. Finally, a few large gaps in the moored temperature and current data were filled by regression with adjacent meters on the same mooring before the seasonal fits, as is described in the Appendix. No filling was done for the wind stress data.

RESULTS

Wind Stress

Figure 2 depicts the mean wind stress vectors, the principal axis ellipses, and the seasonal cycles (annual means included) of the calculated and measured wind stress at each location. A major change in direction of the mean wind stress vectors (from northward to southward) occurs between 40°N and 42°N, near the location (39°N) where the long-term mean marine winds reverse [*Nelson,* 1977]. The ellipses and vector means of the measured wind stresses near the coast line up consistently with the coastline, indicating that the coastal topography redirects the winds near the coast. The ellipses and vector means of the calculated wind stress also tend to be alongshore, but they differ in direction from the measured winds, especially near 40° and 44°N, where the 15° counterclockwise rotation used in calculating the winds from pressure fields appears to be too small [*Halliwell and Allen,* 1984, this issue]. The ellipses of the calculated wind stress in Figure 2*a* are not as narrow as those of the nearshore measurements but are narrower than those of the offshore measurements. The seasonal cycles shown in Figure 2 demonstrate a north-south transition: in the north the strongest winds are the northward winter winds, while in the south they are the spring and summer southward winds.

Figure 3 presents details of the fits of annual (squares) and semiannual (circles) harmonics to the alongshore component of the calculated and measured wind stresses. The vertical lines on the magnitude and phase are estimates of 1 standard error found from the fit statistics, representing approximately a 67% confidence interval. A 95% confidence interval would be about twice as large. These estimates indicate the uncertainty in the magnitude and phase of the harmonics as fit to the given data record. They do not indicate how well these magnitudes and phases represent the long-term seasonal cycle that would be found form a longer (multidecade) record. This is discussed in more detail below.

The magnitude of the annual harmonic of the calculated wind stress is greater in the northern latitudes, with a maximum at 39°–40°N, near the CODE site (Figure 1), and decreases rapidly to the south. This pattern is also evident in the measured wind stress, but the variation between sites obscures it somewhat. The magnitude of the semiannual harmonic shows little systematic change with latitude. The phase of the annual harmonic is approximately the Julian date of its maximum (multiply by $\frac{365}{360}$ and add 365 to negative values), and the phase of the semiannual harmonic has been divided in half so that its value is also close to the Julian date of one of its maxima. The phases are only shown for harmonics which are statistically significant above the 80% level. For the calculated wind stress both harmonics are significant above 95% at all locations, but the semiannual harmonic is only significant at three southern locations for the measured wind stress. At those locations it is significant at the 99% level, and a semiannual nature can be seen in the

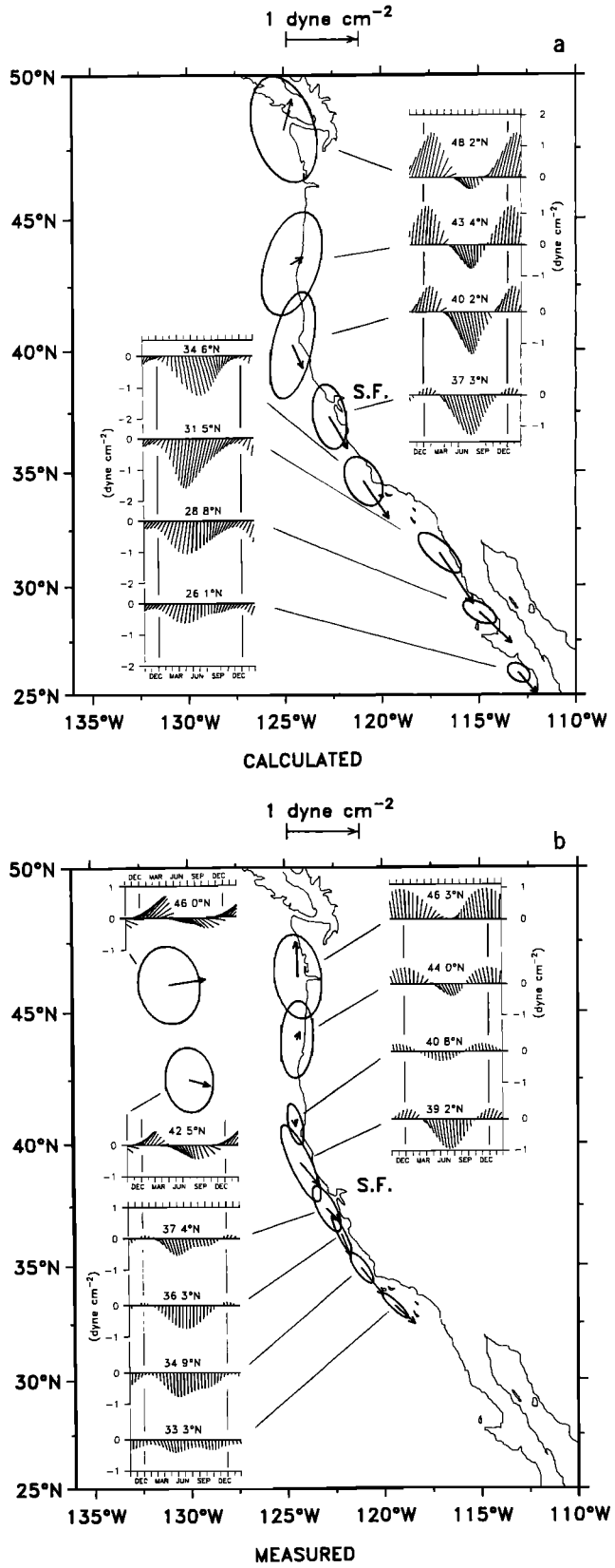

Fig. 2. Annual vector means (arrows), principal axis ellipses, and harmonic-fit annual cycles (stick plots) of the calculated and measured wind stresses. See Table 2 for locations and periods of the data. Ellipses show the principal axes orientation and the standard deviations of the 6-hourly data along major and minor axis components. The scale at the top of the figure applies to the annual vector means and ellipses. Stick plots of the seasonal cycles are oriented so that the vertical axis is parallel to the major axis.

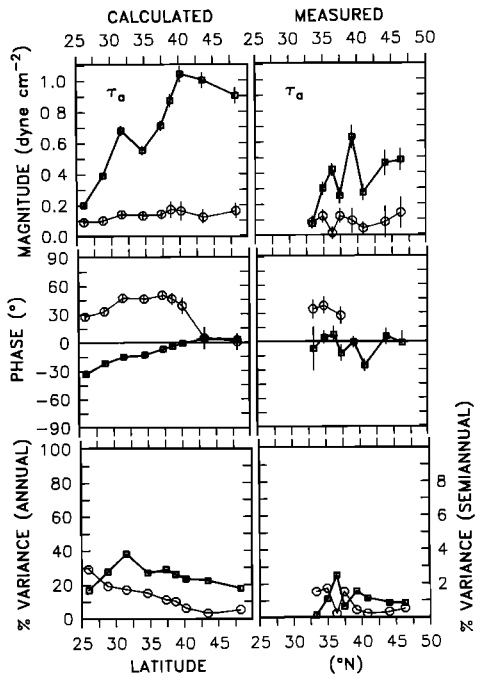

Fig. 3. Latitudinal distribution of statistics of fits of the annual (squares) and semiannual (circles) harmonics to the calculated (left) and measured (right) wind stress. Phases are only shown if the harmonic is significant at the 80% confidence level or greater. The phase of the semiannual harmonic has been divided in half; both annual and semiannual phases correspond roughly to the Julian date of their maxima. The percent variance accounted for by each harmonic is shown at the bottom. The scale for the annual (semiannual) harmonic is on the left (right). Vertical lines represent ±1 standard error estimate in the regression coefficients (67% confidence intervals).

seasonal cycles (33.3°N, 34.9°N, and 37.4°N in Figure 2*b*). The addition of the two harmonics results in a lead of nearly 2 months from south to north of the date of maximum southward calculated wind stress, though the phase of the annual harmonic by itself indicates only 1 month. The phases of the measured winds are less well behaved. The annual harmonic accounts for 17% to 38% of the variance in the calculated wind stress, with a peak in the south at 31.5°N, decreasing to the north. The semiannual harmonic accounts for much less variance, also with a maximum in the south. The less regular statistics for the measured wind show a peak of 25% for the annual harmonic at 36°N and an increased relative importance of the semiannual harmonic in the south.

Figure 4 presents the alongshore wind stress data for 1981 through 1983, with their harmonic seasonal cycles. This figure shows the gaps in the measured data, as well as the alongshore variations in the magnitudes of strong events that may indicate differences in exposure (for example, compare the strength of southward winds in summer 1982 at the four sites from 39.2°N to 46.3°N). The calculated winds, in contrast, are more coherent latitudinally and are usually greater in magnitude than the measured values, both during winter storms in the north and during the summer in the south. Using a constant drag coefficient, *Bakun* [1973] pointed out that the calculated winds overestimate the southward wind stresses in summer near 33°–34°N, which may explain some of the differences between the measured and calculated wind stresses. Use of the variable drag coefficient [*Large and Pond,* 1981] may cause overestimates of the calculated wind stresses during winter storms.

Figure 4 illustrates several features in the data that are not well represented by the harmonic fits. The seasonal cycles do not represent the strong storms that occur during fall and winter in the north. This results in the lower amount of variance accounted for in the north (Figure 3). The energy at these higher frequencies is even greater than indicated by the

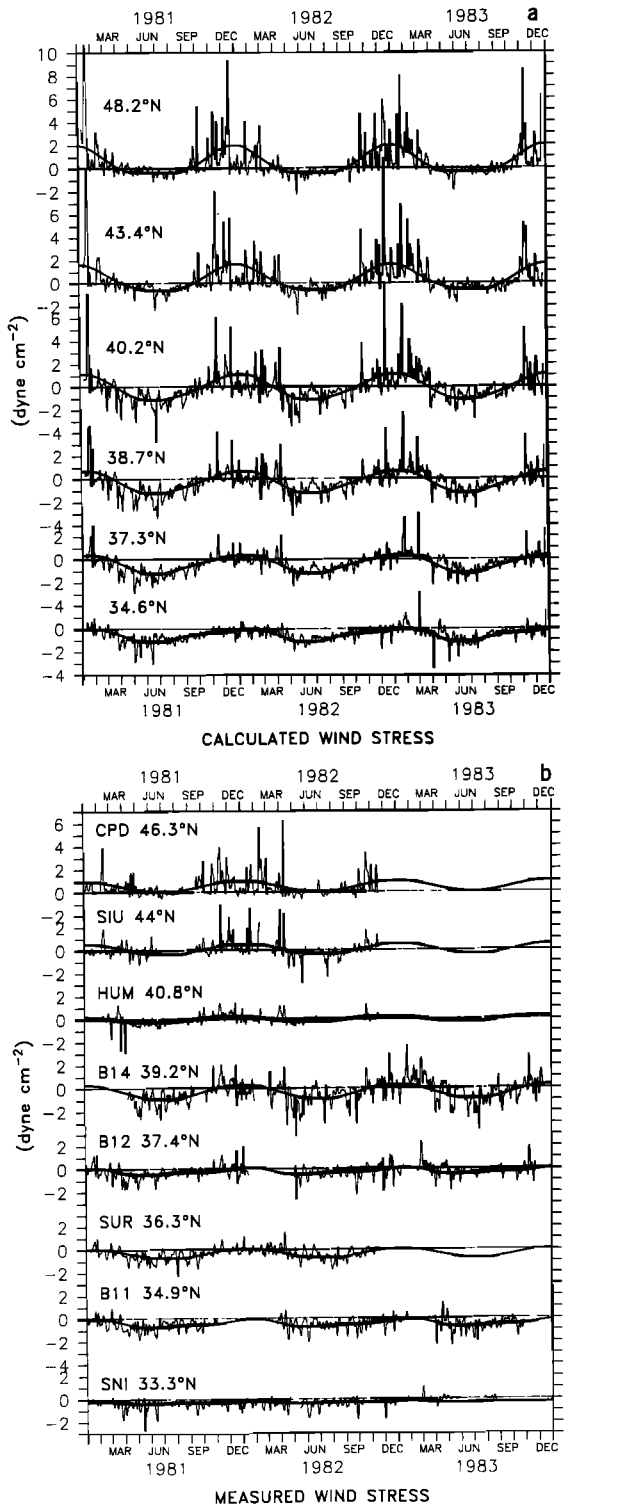

Fig. 4. Alongshore component (along the major axis) of the calculated and measured wind stresses. Figure shows daily values (light line) after application of the LP5 filter (5-day half-power point) and the harmonic-fit seasonal cycle (heavy line).

figures, owing to the use of the LP5 filter before plotting. The sharp transitions in spring and fall are also poorly represented by a harmonic fit. In particular, the 2-month delay between the southern and northern seasonal cycles obscures the fact that a sharp transition can often be seen to occur nearly simultaneously over an extensive north-south domain (for example, from 37°N to 43°N in April 1982, in Figure 4*a*). The large-scale aspects of the spring transition are discussed further by *Strub et al.* [this issue]. The fall transition from summer to winter can also involve a rapid change of regimes, with strong, northward winds of the fall storms replacing fluctuating southward winds (Figure 4*a*, September 1981 at 43°N and 48°N, October 1982 from 40°N to 48°N, and November 1983 as far south as 37°N).

The phase and amplitude of the semiannual harmonic relative to that of the annual harmonic seen in Figure 3 illustrate the ways the semiannual harmonic can manifest itself in the composite seasonal cycles seen in Figures 2 and 4*a*. Where it is in phase with the annual harmonic (Figure 3, 48°N), the composite cycle has a greater and sharper winter peak and a broader summer trough (Figure 4*a*, 48°N). When the phase of the semiannual harmonic lags the annual by roughly 45 days (in the middle latitudes), it spreads the composite peak throughout the winter, provides a sharper decline around day 90, and creates a deeper trough in early spring (Figure 4*a*, 40°N). This approximates the spring transition in the wind stress to the extent possible with only two harmonics. At northern latitudes (38°N to 48°N) the semiannual harmonic's magnitude is only $\frac{1}{10}$ to $\frac{1}{5}$ of the annual's, and the composite cycles do not appear to be semiannual. When the two magnitudes are closer in magnitude, the resultant cycles begin to appear to be semiannual, as is seen most clearly in the calculated wind at 26°N (Figure 2*a*) and in measured winds from 33.3°N, 34.9°N, and 37.4°N (Figure 2*b*). The semiannual nature applies more to the periods of relaxation of the southward wind, with one relaxation around June and a second around December.

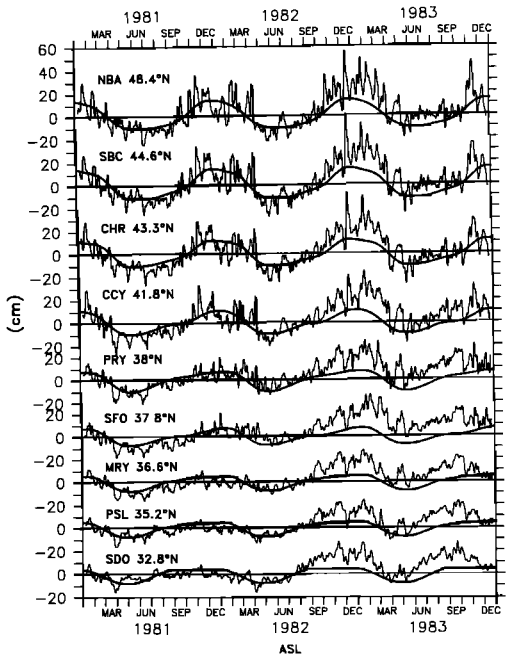

Fig. 5. Adjusted sea level (ASL). Daily (LP5 filter) values (light line) and the monthly average seasonal cycle (heavy line) found from the long-term monthly data (Table 3).

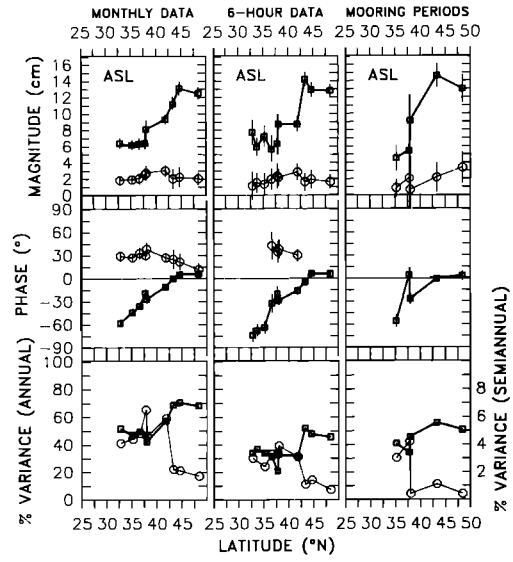

Fig. 6. Latitudinal distribution of statistics of the annual (squares) and semiannual (circles) harmonic fits to ASL: as in Figure 3 for long-term records of monthly data (left), for 4- to 9-year records of 6-hourly data (middle), and for records of 6-hourly ASL, truncated to match the period of the nearest current mooring (right).

Adjusted Sea Level

The annual cycles of the long monthly ASL records (typically 1950–1983; see Table 3) were found by averaging calendar months as well as by fitting harmonics. The average monthly cycles are presented in Figure 5 along with the filtered 6-hourly data for 1981–1983. For these long records, fits to two harmonics are very similar to the average monthly cycles, as is discussed in the second part of the appendix. Details of the fits of the monthly data to the two harmonics are presented in Figure 6 on the left. Details of the fits of the 4 to 9 years of 6-hourly data are presented in the middle column. To assess the influence of the individual mooring periods on the harmonic fits to the current and temperature data presented below, we truncated the 6-hourly ASL data from stations closest to the current moorings to match the periods of the current records and recomputed the first two harmonics; these are also shown in Figure 6 on the right.

A comparison of Figures 5 and 6 to Figures 3 and 4 indicates that many features of the ASL records are similar to those of the calculated and measured wind stresses. In Figure 5 the low period in the ASL seasonal cycles begins earlier in the south, with a lag of ~2 months in the north. Both harmonics are significant at the 95% level for the long monthly ASL records, and their magnitudes and phase relationships show the same qualitative north/south behavior as the wind stress. In the north the two harmonics are in phase, combining to form a narrow winter peak and broader summer trough (for example, 48.4°N in Figure 5). In the middle latitudes the annual harmonic peak is earlier, the semiannual harmonic is later, and the combined seasonal cycle has a broad peak, narrow trough, and sharper transition (for example, 38°N in Figure 5). In the south the magnitude of the first harmonic (Figure 6, top) is low and nearly constant from 32°N to 37°N, rising to values twice as

large at 45°N and 48°N. The semiannual magnitude is maximum in the middle latitudes (38°N to 42°N), where a slight semiannual periodicity can be seen in the more rapid rate at which the ASL rises around June and again around October (for example, 41.8°N in Figure 5). For the shorter (4 to 9 years) records of 6-hourly ASL (middle column of Figure 6), the region between 36.6°N and 41.8°N is the only region where the semiannual harmonic is statistically significant at the 80% level. The amounts of variance accounted for by the seasonal cycles of the 6-hourly ASL data (Figure 6, middle column) are generally greater than those accounted for by the 6-hourly wind stress cycles (Figure 3). The annual harmonic of ASL accounts for approximately 50% of the total variance in the north and 30% in the south, with a sharp transition region between 38°N and 43°N. This is unlike the wind, which rises steadily from less than 20% at 48°N to nearly 40% at 32°N. The semiannual harmonic accounts for more variance (3 to 6%) in the middle latitudes.

In Figure 5 the high sea levels associated with the 1982–1983 El Niño are evident from 33°N to 48°N. These high sea levels began in September 1982 in the south and in October 1982 in the north. Greater than normal northward coastal winds (Figure 4) were also associated with the El Niño, but only after December 1982. *Huyer and Smith* [1985] suggested that the high sea levels during October and November off Oregon were connected to high sea levels off Peru via an oceanic path, with about a month between high sea levels at the equator and those off Oregon. The data presented here show that their observations apply to the entire coast from 33°N to 48°N.

The comparison between the far left and far right columns of Figure 6 is the best test of whether the periods of the current and temperature records allow an estimate of annual cycles that are representative of the seasonal cycles that would be found from much longer records. The annual harmonics for the mooring periods are similar in magnitude to those for the full ASL data set, with slightly greater magnitudes in the north (39°–48°N) and lesser magnitudes in the south (35°–37°N). The phases are very similar, except near 37°N, suggesting that the mooring period should yield representative annual cycles of currents and temperatures, except possibly at the H3 mooring (see below). The semiannual harmonic was not significant at the 80% level for fits to the mooring period ASL, which suggests that significant semiannual harmonics found in fits to the current and temperature records are not caused by the mooring period alone but are characteristics of those records.

Currents

The principal axis ellipses and annual mean current vectors for the top and bottom sensors of each mooring are shown in Figure 7 and listed in Table 1. The principal axis ellipses and means were calculated for 1 full year—May 1, 1981, to May 1, 1982—common to all current records. The seasonal cycles of current vectors for all sensors (except H3) are presented in Figure 8. These cycles were found by fitting the harmonics to alongshore and cross-shelf components of the current separately, for the complete data periods listed in Table 1.

The mean currents and ellipses measured by the lowest instruments, 18–60 m above the bottom, (Figure 7, on the right) demonstrate the strong control of the bottom topography (Figure 1). Many of the bottom ellipses are narrower

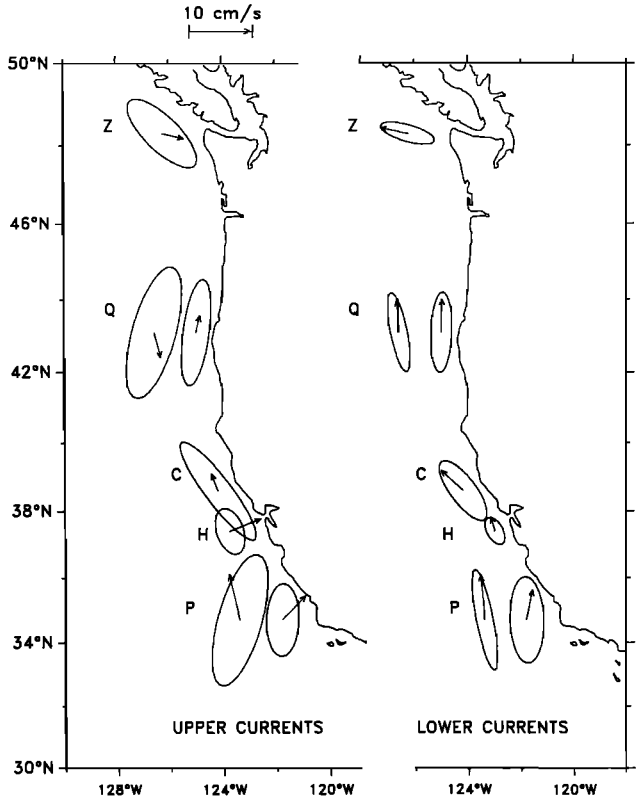

Fig. 7. Annual vector means (arrows) and principal axis ellipses, calculated from 1 complete year of 6-hourly current data (May 1, 1981, to May 1, 1982), for the top and bottom instruments on each mooring. The centers of the ellipses are at the latitudes of the moorings (Table 1), but the longitudinal positions have been displaced for better viewing.

than those from 35 m, and all bottom instruments show poleward mean alongshore flow. At the upper instrument the annual mean flow is more variable in space. Over the shelf break the upper level currents are southward at 48°N and 43°N and northward at 35°N, opposing the annual mean wind stresses at the same locations. Over the midshelf the mean upper level currents are primarily northward. The onshore components at 35°N and 37°N may reflect the fact that winds are southward and are upwelling favorable on average, with onshore flow at 35 m compensating the mean offshore Ekman flow at the surface. Alternately, the moorings may have been located in a semipermanent eddy or gyre caused by local topography. We have neither the horizontal nor the vertical resolution to determine the correct explanation.

From past measurements off Oregon at 45°N we expect the seasonal cycle to alternate between a winter regime with mean northward, barotropic flow and a spring-summer regime with mean southward, strongly sheared flow [*Huyer et al.*, 1979]. This structure is observed in Figure 8 at the shelf break at 48°N and 43°N. At 43°N the southward flow over the midshelf is of shorter duration than at the shelf break. The southward summer midshelf currents at 39°N are weak but of longer duration than those over the midshelf at 43°N. At 35°N, southward currents over both the midshelf and shelf break occur for only a brief (2 months) period in spring. The mean northward flow in winter appears to be nearly barotropic at all locations. A semiannual cycle is evident in the northward currents at 35°N, with maxima during July and January, similar in phase to that found by *Chelton* [1984]

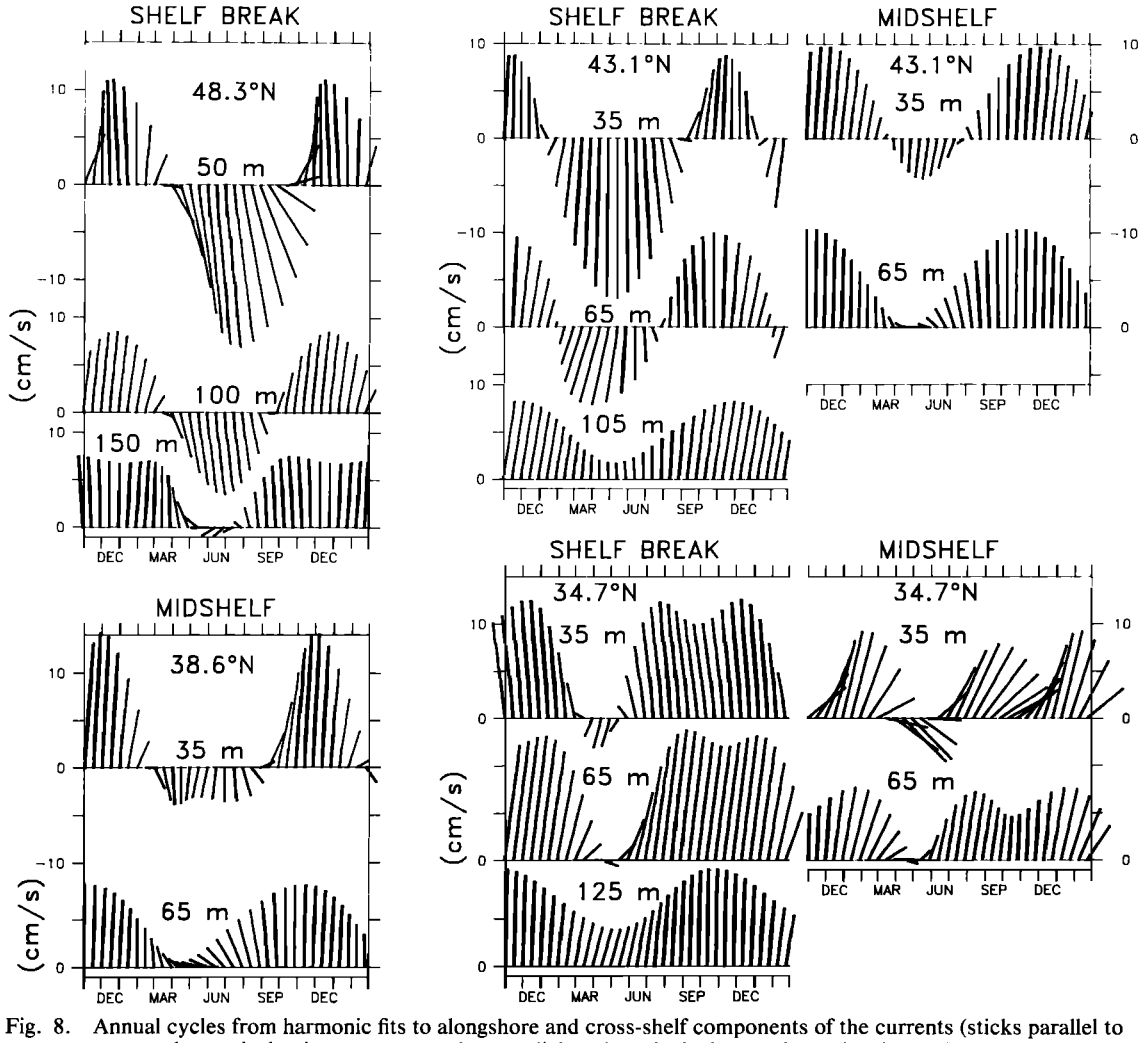

Fig. 8. Annual cycles from harmonic fits to alongshore and cross-shelf components of the currents (sticks parallel to the vertical axis represent motion parallel to the principal axes shown in Figure 7).

in the northward geostrophic undercurrent at the same latitude. The fit to the semiannual harmonic is significant at greater than the 99% level for the data from the midshelf currents at 35°N, at the 82–96% level for the shelf break currents at 35°N and the midshelf currents at 39°N, and below the 80% level elsewhere.

Details of the harmonic fits to alongshore currents (Figure 9) show clearer north-south patterns at the three shelf break moorings than at the four midshelf moorings. The north-to-south decrease in the magnitude of the annual harmonic is similar to that seen for alongshore calculated wind stress and ASL. The increase in the absolute magnitude of the semiannual harmonic seen at 35°N for the current data (Figure 9) was not seen in calculated wind stress and ASL (Figures 3 and 6). For those data, only the relative magnitude was greater in the south, owing to the decrease in the magnitude of the annual harmonic. The south-to-north lead seen in the phase of the annual harmonic at the shelf break is similar to that of the ASL. The midshelf phase relationships are similar to those at the shelf break, if one ignores the midshelf data from H3 (37.4°N), as is suggested by the truncated ASL data in Figure 6. Both currents and ASL lead the wind stress at all latitudes by 1 or 2 months, and currents lead ASL at some latitudes by 1 month or less. The percent of variance accounted for by the annual harmonic is quite low (7–12%) over the midshelf, and only slightly greater (14–17%) over the shelf break, except at 48°N where it is 53%. Below 35 m (not shown) the amount of variance accounted for by the seasonal cycles decreases with depth at all except one station (35°N at the shelf break).

Fits to the weak cross-shelf currents (not shown) account for even less of its variance, usually less than 3%, but do show a north-to-south decrease in the annual harmonic magnitude. Over midshelf the magnitude of the semiannual harmonic increases from north-to-south, as it does for the alongshore currents. The phase of the cross-shelf annual cycle is between 0° and −60° over midshelf, indicating maximum onshore flow in the fall and offshore flow in the spring.

Time series of the alongshore component of the midshelf (shelf break at 48°N) upper current are presented in Figure 10, along with their annual cycles. This figure clearly shows that most of the variability cannot be accounted for by the annual cycles, except at the 48°N (shelf break) location. *Freeland et al.* [1984] used a 3-year record of currents from the same 48°N location to argue that the seasonal cycle off Vancouver Island is so regular that 1 year's data is representative of the average annual cycle. Except at the 48°N shelf break location the summer regime during these years does not consist of the persistently southward currents

expected from the 1973–1974 data from midshelf at 45°N [*Huyer et al.*, 1979]. Even at 48°N, monthly mean data from the midshelf moorings in 1980 and 1981 show that the currents inshore of the shelf break mooring presented here are weakly northward in summer [*Freeland et al.*, 1984]. Over the shelf break at 43°N (not shown) the southward currents are slightly more persistent than the midshelf currents shown here but not like those at the shelf break at 48°N nor like the earlier data from 45°N, which showed persistent southward flow from late March into October. In the present data from 43°N, the difference between the midshelf and shelf break currents is subject to some uncertainty because the "35-m" instrument over midshelf was sometimes as deep as 51 m (spring 1981) and was usually 6 to 7 m deeper than the corresponding shelf break instrument. From July 1983 on, however, the top midshelf instrument at 43°N was maintained at 35 m depth, and the current record during the summer of 1983 reverses direction as often as during the previous summer. Thus the currents at both midshelf and shelf break at 43°N are qualitatively different from those at the shelf break at 48°N during this experiment and different from those at midshelf at 45°N during previous experiments. At 35°N the shelf break currents are similar to the midshelf currents shown; both have only a short period of southward flow in the spring. The magnitudes of the short-period fluctuations are greatest at 43°N and 39°N, but at 43°N there appears to be a seasonal decrease in the magnitudes during summer, while at 39°N the fluctuations maintain their strength all year. At 37°N the magnitudes of fluctuations and seasonal currents are all much less than elsewhere.

At 43°N the magnitudes of the northward currents increase during the winter of El Niño, 1982–1983. This can be seen more clearly in the monthly averages presented in the discussion section below and by *Huyer and Smith* [1985].

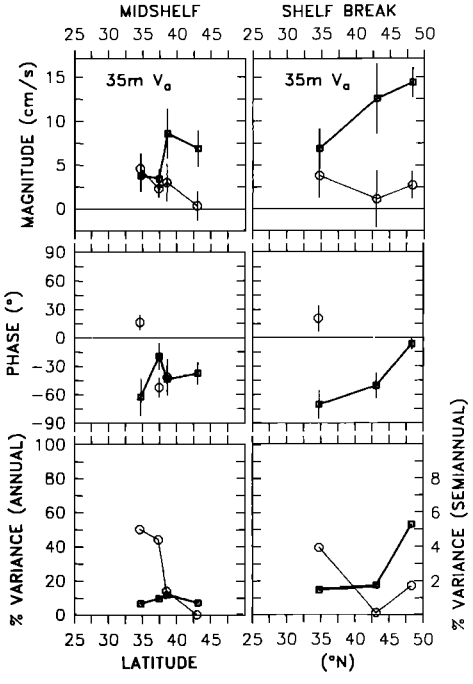

Fig. 9. Latitudinal distribution of statistics of the annual (squares) and semiannual (circles) harmonic fits to the 6-hourly alongshore currents at the upper current meters: as in Figure 3 for 35-m currents from over (left) the midshelf and (right) the shelf break.

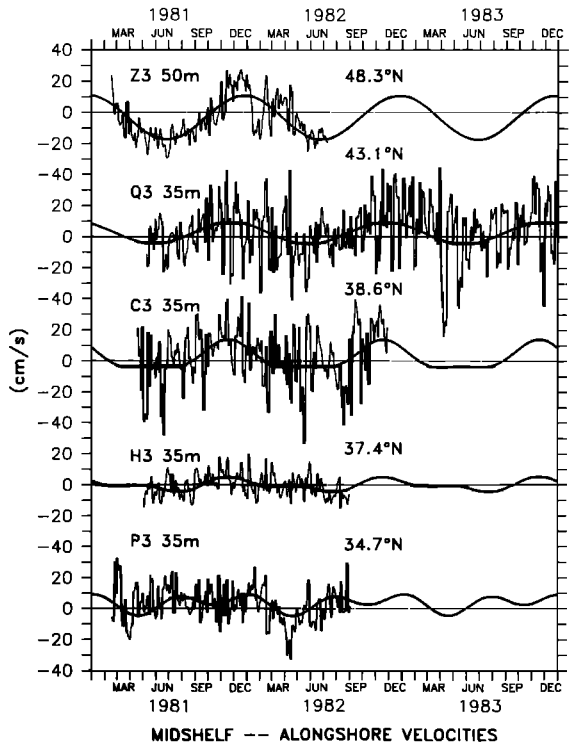

Fig. 10. Alongshore velocities. Daily (LP5 filter) values of midshelf alongshore (major axis) velocities at the upper instrument on each mooring (light line) and harmonic fit seasonal cycles (heavy line). The semiannual harmonic is significant and included only at 38.6°N, 37.4°N, and 34.7°N.

In Figure 8 the vertical shears in the seasonal cycles of currents over the shelf break at 48°N and 43°N generally agree with past observations made off Oregon and Washington. The vertical shear of the alongshore component of the shelf break currents at 43°N and 35°N are shown in Figure 11 (upper curve in each panel). Harmonic fits to the data are also shown; in this case the unfilled data records were used, since most of the filling was done by regression between instruments on the same mooring. Differences in sensor depth on different mooring deployments have only a small effect on the shear calculations, since the sensor separation varied by less than 8% of the separation distance. At the shelf break the shear at 43°N follows the pattern expected from previous data, as it does at 48°N (not shown): shear is negative during the summer and near zero (on average) during the winter. Fluctuations in the currents during summer are more barotropic in nature and weaker than they are from October to June. Over the midshelf from 37°N to 43°N (not shown), the same pattern can be seen, but it is much weaker and less persistent than at the shelf break at 43°N. To the south at 35°N over the shelf break, the period of persistent negative shear is limited to the spring period of the southward currents; during the summer and fall the shear fluctuates about a slightly positive mean (the upper meter failed during the winter). Over the midshelf at 35°N (not shown), the vertical shear consists of short-period fluctuations about a near-zero mean throughout the entire year.

At 35°N and 43°N it is possible to look at the relation between the vertical shear at the shelf break and the horizontal temperature gradient from midshelf to shelf break. The temperature difference between the midshelf and shelf

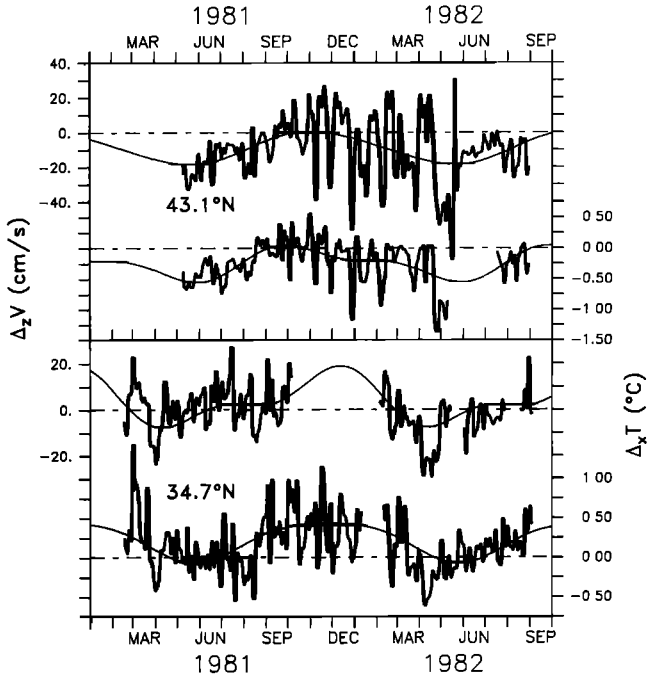

Fig. 11. Vertical difference in the alongshore velocity compared to horizontal cross-shelf temperature difference at (top) 43°N and (bottom) 35°N. Daily values of the alongshore velocity difference (heavy line) between the upper (35 m) and lower (~130) current meters at the shelf break are shown at the top of each panel, along with two-harmonic fits to the same data (light line). Similar daily values and two-harmonic fits are shown for the cross-shelf temperature difference at ~70 m (midshelf minus shelf break) at the bottom of each panel.

break moorings at about the 70-m depth is shown as the bottom curve in the two panels of Figure 11. If salinity were not important in determining the density, the comparison would serve as a test of cross-shelf geostrophy, as is represented by the thermal wind equation. Differences in instrument depth on different deployments affect the cross-shelf temperature differences to a greater extent than they do for the shear and may cause a change of 0.1°C to 0.4°C in background bias between deployments. Even with these errors the seasonal cycles and short-term fluctuations of shear and temperature difference are similar to each other at both latitudes, except for the artificial second harmonic in shear at 35°N, which is caused by the large data gap. The correlation coefficients between the 6-hourly values of vertical shear and cross-shelf temperature difference are 0.78 at 43°N and 0.63 at 35°N. With the seasonal cycles removed, these decrease only slightly to 0.74 at 43°N and 0.60 at 35°N, both significant at the 99% level and comparable to correlations found by *Huyer et al.* [1978] at 45°N using horizontal density differences.

Temperatures

The temperature time series shown in Figure 12 have much less short-term variability about the seasonal cycle than the other variables discussed and are characterized by large-magnitude abrupt transitions, especially in spring and fall. The drop in temperature seen in spring (for example, April 1982) appears strongest in the middle of the domain from 37°–43°N. The cool temperatures in spring and summer are much more persistent than the southward currents seen in Figure 10 and resemble the ASL records from spring through fall. The transition to warmer temperatures in fall is most abrupt at 43°N (October of all 3 years), where the fall transition influences the seasonal cycle more than the spring transition. This is seen in the statistics of the seasonal cycle at 43°N (Figure 13), where the phase of the midshelf semiannual harmonic is approximately −60° (day 300, early November), which results in a rapid rise in the fall, a behavior not seen in the other variables. After the fall maxima, temperatures decrease in winter to values slightly above their annual averages, prior to the next spring transition. An exception to this winter cooling occurred during the 1982–1983 El Niño at 43°N, where the 35-m temperature stayed warm through March 1983. North of 43°N and south of 37°N, there is a change from the rapid spring and fall transitions to more gradual transitions and weaker annual cycles. The shelf break data from 35 m depth at 43°N and 35°N (not shown) are similar to those at midshelf. The temperatures from the lowest instruments on all the moorings (not shown) are also similar but have a slightly more abrupt spring transition to cold water, reaching their coldest temperatures right after the transition, without the approximate month delay seen at the top sensors (for example, April–May 1982 in Figure 12). *Strub et al.* [this issue] show details of the temperature changes during the spring transition along the coast.

The greater range of the annual cycles at the middle latitudes is seen in the magnitude of the annual harmonic in Figure 13. There is a slight maximum in the semiannual harmonic at 43°N, where it approximates the fall transition,

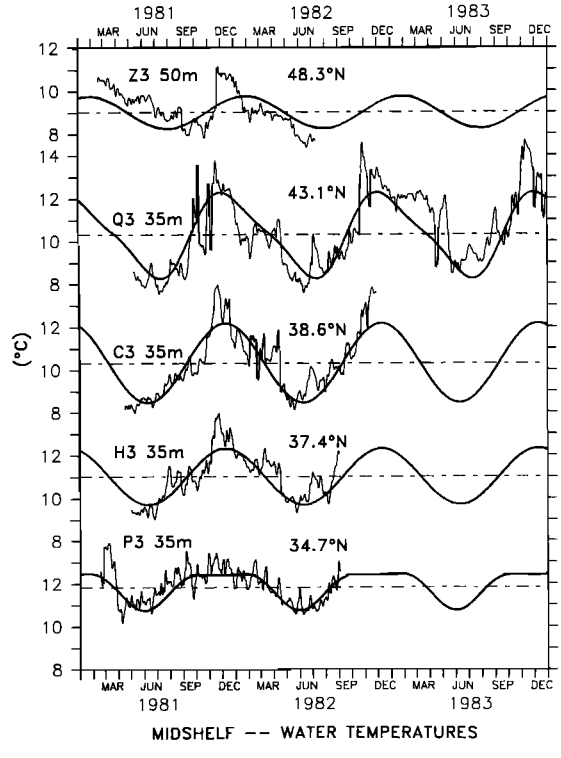

Fig. 12. Water temperatures at the upper meter on the midshelf moorings (shelf break at 48°N). Daily (LP5) values (light line) and the harmonic-fit seasonal cycles (heavy line) are shown. Only the seasonal cycles from 43.1°N and 34.7°N include the semiannual harmonic.

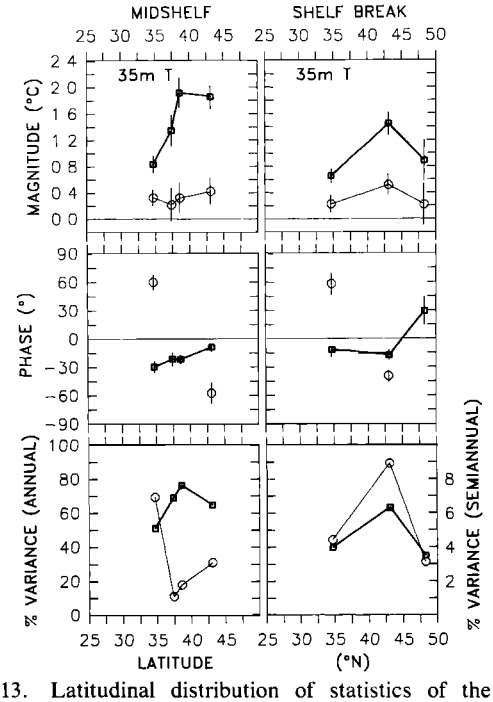

Fig. 13. Latitudinal distribution of statistics of the annual (squares) and semiannual (circles) harmonics of the temperature data at 35 m: as in Figure 3 for data from over (left) the midshelf and (right) the shelf break.

and also at 35°N over the midshelf, where it produces the flat winter peak. These are the only two locations where the semiannual harmonic is significant above the 80% level. Over midshelf a south-to-north lead is indicated by the phase of the annual harmonic in Figure 13 and can be seen in Figure 12. There is a similar south-to-north lead in the seasonal cycles at the shelf break (not shown). The phase of the temperature seasonal cycles are similar to those of the winds, lagging those of currents and ASL. The amount of variability accounted for by the annual harmonic varies from 51% to 76% at midshelf and from 34% to 64% at the shelf break. Unlike the alongshore currents the amount of variance accounted for by the seasonal cycle does not decrease from shelf break to midshelf nor does it decrease with depth.

Discussion

Large-Scale Structure of Seasonal Cycles in the Coastal Ocean

Figure 14 summarizes the results by presenting the seasonal cycles of each variable at the four locations with the most complete data. The measured winds shown for the 48°N site are actually from 46°N (CPD in Table 2), but at the other locations the measured winds (SIU, B14, and B11 in Table 2) are from the same latitudes as the currents, temperatures, ASL, and calculated wind stresses. In general, Figure 14 shows that southward (or less northward) winds and 35- to 50-m currents are associated with low ASL and water temperature for a period in spring and/or summer, and the opposite is true for some period in the fall and/or winter. The currents lead ASL slightly, and both lead the wind and temperature. The lead of currents over wind stress is seen most clearly in the timing of the onset of the spring and summer regimes. A south-to-north lead of approximately 2 months can be seen in the spring-summer minima of all the variables. The southward currents in spring and summer have a baroclinic shear (Figures 8 and 11), such that deeper currents are northward, or more weakly southward. At 43°N this shear is more persistent at the shelf break than over the midshelf. At the southern end of the domain (35°N) this southward, sheared regime is compressed into a 1- to 3-month period in spring, and a semiannual peak is seen in northward alongshore current, roughly coincident with the two periods when measured wind stress weakens rapidly. At the northern end of the domain (48°N) at the shelf break, the summer and winter current regimes are equal, and the seasonal cycle is very regular.

The measured wind stress data confirm that the magnitude of the seasonal cycle of alongshore wind stress has a maximum around 39°–40°N and that the mean wind stress switches at this latitude from northward (in the north) to southward (in the south). Although this has been reported previously on the basis of calculated (pressure derived) winds [*Bakun*, 1975] and marine weather reports [*Nelson*, 1977], confirmation by measured winds from well-maintained anemometers has not been available previously. In contrast to the wind stress, southward currents during the summer are strongest and most persistent at the shelf break in the north (48°N) where the southward winds are weakest,

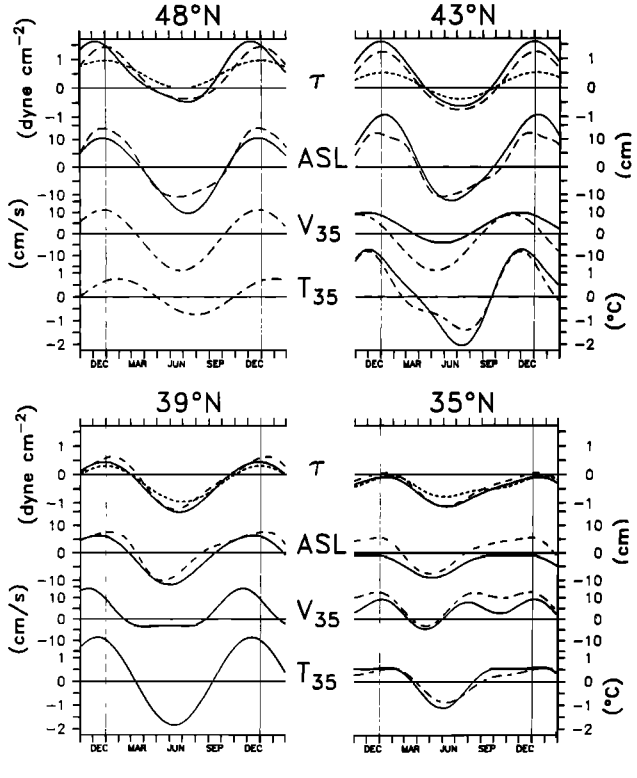

Fig. 14. Seasonal cycles of alongshore wind stress, ASL, alongshore water velocity, and temperature at 35 m depth. The three curves for alongshore wind stress (τ) show the harmonic fit to the calculated wind stress that has been truncated to match the mooring period at that latitude (solid curve), the fit to the complete 4–9 years of 6-hourly calculated wind stress data (long-dashed curve), and the fit to 1–3 years of 6-hourly measured wind stress records (short-dashed curve). The two curves for ASL show the two-harmonic fit to the 6-hourly data truncated to match the mooring period (solid curve) and the long-term monthly average seasonal cycle (dashed curve). The solid curves for alongshore water velocity (V_{35}) and temperature (T_{35}) represent the harmonic fits to the upper midshelf 6-hourly current meter data; the dashed curves represent the upper shelf break data.

and northward currents are strongest and most persistent in the south (35°N) over both midshelf and shelf break where northward winds are very rare. In the middle of the domain (39°N to 43°N), where the seasonal cycle of wind stress is observed to be strongest, the seasonal cycle of currents is weaker than farther north and is nearly obscured by large-amplitude short-term fluctuations. Thus the strength of the seasonal cycle in the alongshore currents is not a simple function of the strength of the seasonal cycle of local alongshore wind stress.

The present results provide a latitudinal context for previous observations. The historical current data from the midshelf off Oregon, such as the long 1973–1974 record from Station Poinsettia (45°N) shown by *Huyer et al.* [1979], are similar to the shelf break currents reported here at 48°N. Harmonic fits to the Poinsettia 40-m alongshore currents result in a magnitude of ~20 cm/s for the annual harmonic, larger than those found during 1981–1982 at the shelf break at 43°N (13 cm/s) or 48°N (14 cm/s). If included in Figure 9, this would result in a maximum range in the seasonal cycle of alongshore current at 45°N, which would make the latitudinal variation of the annual magnitude similar to that of ASL. The amount of variance accounted for by the annual harmonic is 36% at Poinsettia, fitting between the 17% at 43°N and 54% at 48°N. The phase at Poinsettia is −21°, which also falls between −51° at 43°N and −6° at 48°N. Thus although Poinsettia was a midshelf mooring, it fits reasonably well into the shelf break distribution between 43°N and 48°N, resulting in an alongshore current pattern like ASL. This suggests that a transition region may exist between 43°N and 48°N, with a decrease in the role of higher-frequency fluctuations as one moves north of 43°N, until the regular seasonal cycles account for more of the variance than the fluctuations. An alternate possibility is that the 1973–1974 and the 1981–1982 periods experienced different conditions over the shelf, but this possibility seems unlikely: data from a midshelf mooring (Sunflower) at 45°N in 1975, presented by *Huyer et al.* [1979], show a persistently southward summer current regime at 45°N during that year also, supporting the idea that this is the normal situation at 45°N. At 43°N the 1981–1983 current record allowed observation of the energetic midshelf fluctuations during three summers (Figure 10). Thus the available data support the presence of a spatial difference, rather than a temporal difference, in the behavior of the currents at 43°N and 45°N.

At 35°N the previous description of the seasonal currents presented by *Chelton* [1984] is based on geostrophic velocities calculated from historical hydrographic observations off Point Conception. At the most inshore location (still offshore of the 500-m isobath), Chelton found southward surface currents from March through September and northward surface currents from October to February; at a depth of 150 m the geostrophic flow was northward all year, with maxima in June and December. This semiannual variation in the undercurrent is similar in phase to the semiannual signal we observed at depths of 35 m and 65 m over the shelf, i.e., maxima in late July and December (Figure 8). This coincidence in phase suggests that the northward flow in the undercurrent may extend up over the slope onto the shelf. Direct current measurements over the slope are not available for 1981–1982, but nine conductivity, temperature, and depth sections were made between February 1981 and February 1984, and the dynamic topography of these sections was extrapolated onto the shelf using the method of *Reid and Mantyla* [1976] to obtain geostrophic velocities relative to 500 dB. Sections from late April through January (five sections) all show northward flow over the shelf and slope and southward flow farther offshore (except in January, when flow is still northward farther offshore); three February sections and one early April section all show southward currents over the shelf and slope. The generally northward flow over the shelf is in contrast to the southward spring and summer geostrophic flow found by Chelton over the slope and suggests that his results should not be extended to the region over the shelf. More detailed hydrography from over the slope and shelf between 35°N and 36°N has recently shown both the northward flow over the shelf and the southward surface flow farther offshore in February, July, and October 1984 and January 1985 [*Chelton et al.*, 1986] to be in agreement with our observations. Alongshore geostrophic transport near the coast at 36°N [*Wickham et al.*, 1986] in 1979–1980 also shows a similar pattern of generally northward transport during the year except for a brief period of southward transport in early spring, with the suggestion of a semiannual peak in northward transport. These data support the idea that the northward current seen over the shelf from May through January is part of the same current seen at depth farther offshore and may experience the same semiannual peaks. The hydrographic data from late April 1981 and May 1982 show this northward flow extending to the surface, though winds were southward. The same event is seen here in the reversal of 35-m currents over the shelf from southward to northward in April 1981 and in May 1982. The combined data suggest that the return to northward flow opposing southward winds, after a brief period of southward flow in spring, is a common occurrence at 35°N, though its cause is unknown.

Assessing the 1981–1982 Period

How representative are the seasonal cycles presented above, considering the length of the 1981–1982 period of data? One indication is seen in Figures 6 and 14 by comparing fits of 6-hourly ASL data, truncated to match the period of the nearby mooring (solid line in Figure 14 ASL cycles), to the long-term average monthly seasonal cycles (dashed line in Figure 14). The fits to the mooring periods are similar to the long-term fits, with a tendency to have a later and lower spring minimum. The greatest difference caused by use of the mooring period data occurred at 37°N (Figure 6), where the phase of the annual harmonic changed greatly and the magnitude decreased. The magnitude of the annual harmonic at 35°N was also decreased by use of the mooring period, suggesting that the weaker currents measured at those moorings may underestimate the usual seasonal cycle.

By using the same method to assess the measured wind period, the nearest calculated wind stress record was truncated to match each of the measured wind stress periods (including gaps), and harmonic fits were performed. The resulting seasonal cycles (not shown) were virtually identical to the cycles found from the full 9 years of calculated wind stress data. The only visible differences were found north of 39°N, where northward wind stress in the fall was slightly stronger and occurred earlier than in fits to the full records. These comparisons suggest that the period of wind measurement was generally representative and that differences between the seasonal cycles of the measured and calculated

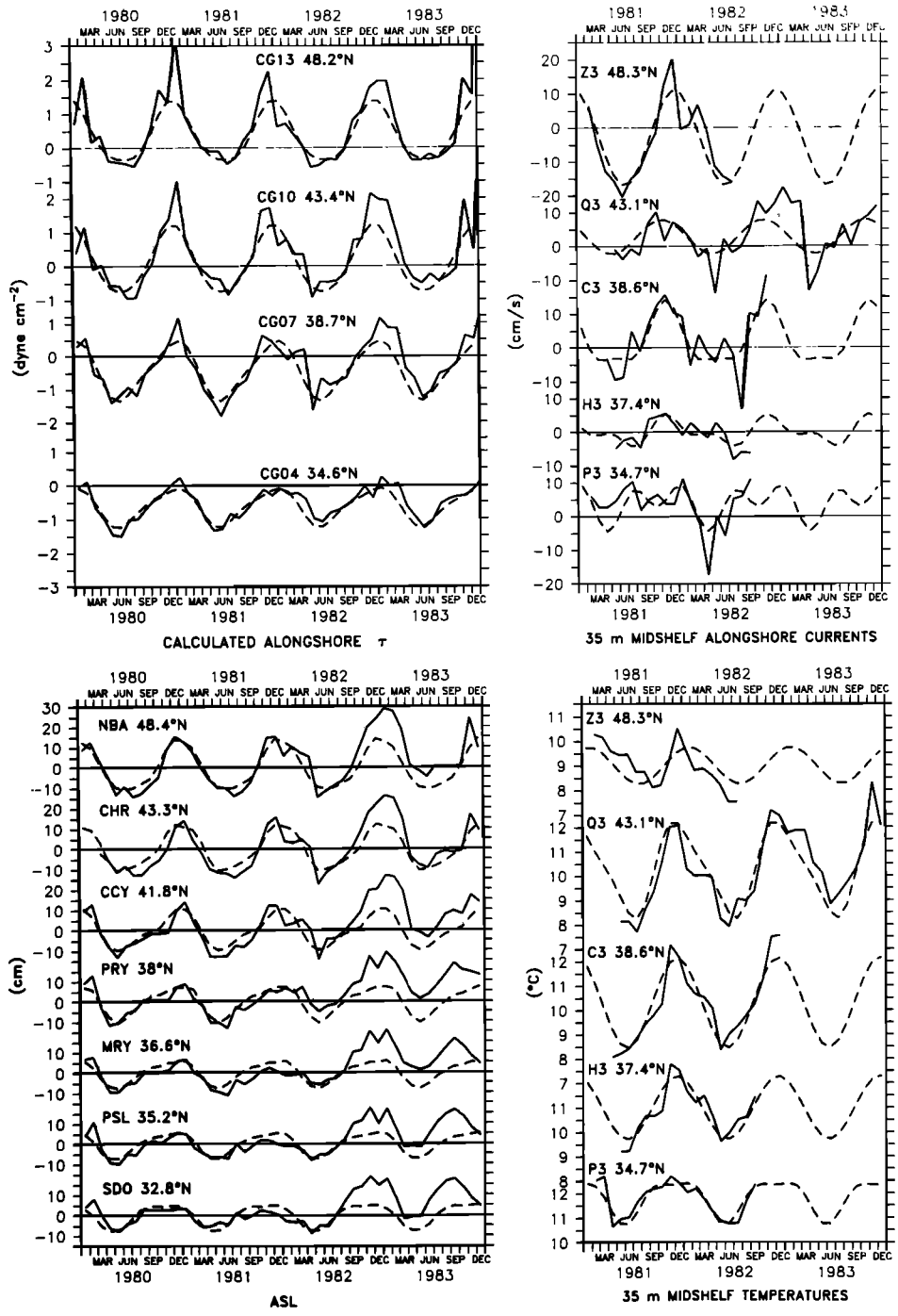

Fig. 15. Monthly mean values (solid lines) of calculated alongshore wind stress (top left), ASL (bottom left), midshelf (shelf break at 48°N) alongshore 35-m currents (top right), and temperatures (bottom right). All monthly values are monthly means of the 6-hourly data, the seasonal cycles of ASL (dashed lines) are the long-term monthly averages, and the other seasonal cycles are harmonic fits to the 6-hourly data.

wind stress are not caused by the measurement period but by real differences in the data. In particular, the semiannual nature of the relaxation of the measured wind stress in the south was probably not caused by peculiarities of the measurement period. In order to examine the wind forcing during the mooring periods, the calculated wind stresses were truncated to the mooring periods and the seasonal cycles found again. These cycles are shown as the solid lines in Figure 14 and are again nearly identical to the seasonal cycles found from the full 9 years of data, shown by the long-dashed lines. The major difference is a tendency to have a slightly earlier and greater fall peak in the north, similar to that found when the calculated wind stress records were truncated to match the measured wind stress periods.

A summary of the year to year variability in the seasonal cycles is shown in Figure 15, where monthly means of all data are displayed against their seasonal cycles. The difference between the individual monthly values and their normal seasonal values shows the interannual variability. The variability with time scales less than a month is presented in

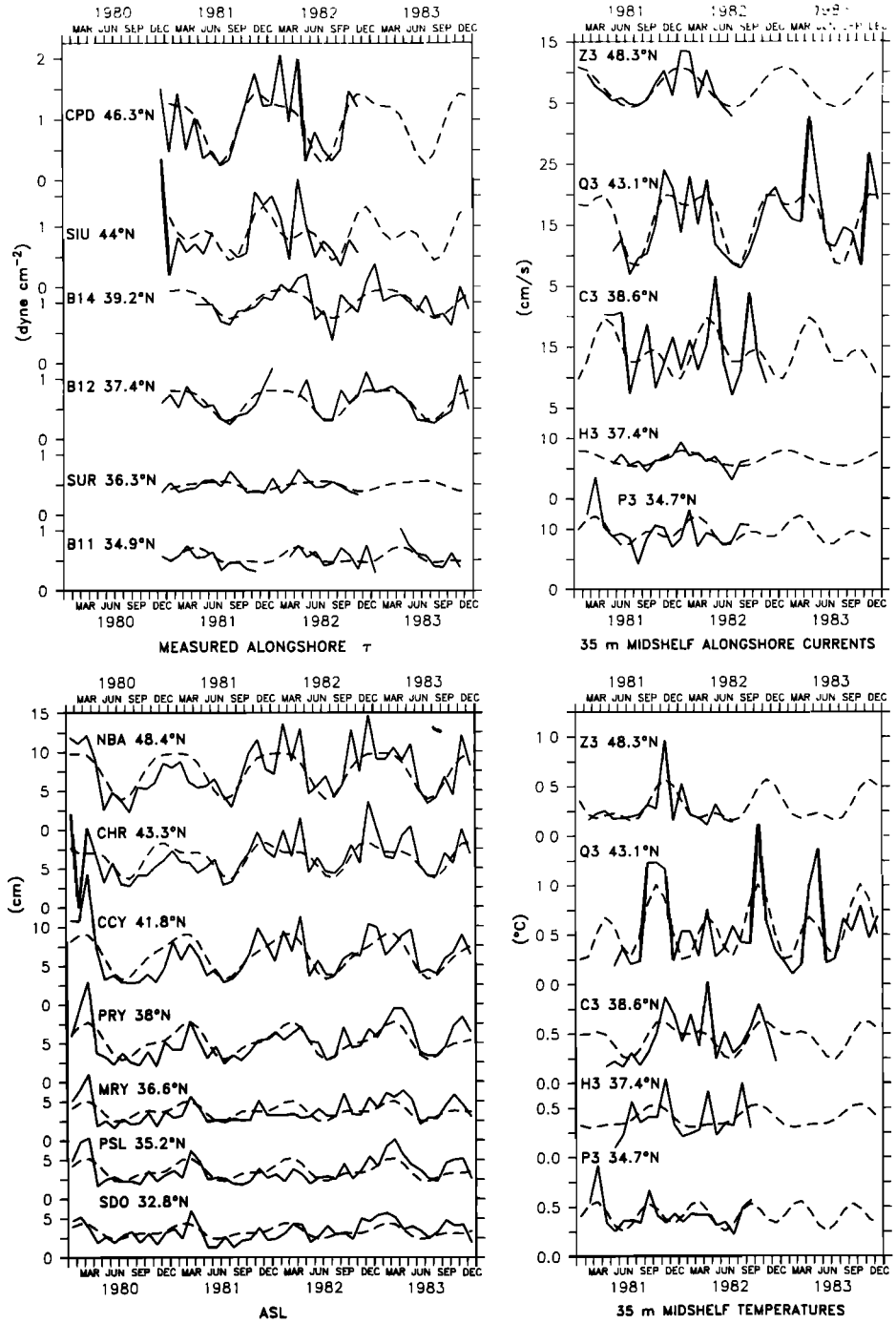

Fig. 16. Monthly standard deviations (solid lines), derived from 6-hourly data, for measured alongshore wind stress (top left), ASL (bottom left), midshelf (shelf break at 48°N) alongshore 35-m currents (top right), and temperatures (bottom right). The dashed lines are harmonic fits to the monthly standard deviations. Two harmonics were used, regardless of significance.

Figure 16 by plotting the monthly standard deviations of the 6-hourly data, along with harmonic fits to these monthly standard deviation values. Standard deviations of measured wind stress are shown instead of the calculated wind stress, because the calculated wind stress tends to overestimate the wind stress during winter storms, producing the pattern seen in Figure 4*a*. This results in 1 month with a sharp spike of standard deviation each year due to the exaggerated values of stress found during the one or two strongest storms each year. Standard deviations of the measured wind stress are less dominated by single events and appear more similar to the standard deviations of ASL. The monthly mean data (Figure 15) make the seasonal nature of the data more evident, while the standard deviations of the shorter fluctuations themselves display a seasonal nature, especially in the north (Figure 16).

In order to help assess the significance of differences between the monthly values of calculated wind stress and ASL and their seasonal cycles, the monthly anomalies are plotted in Figure 17 (the difference between the monthly

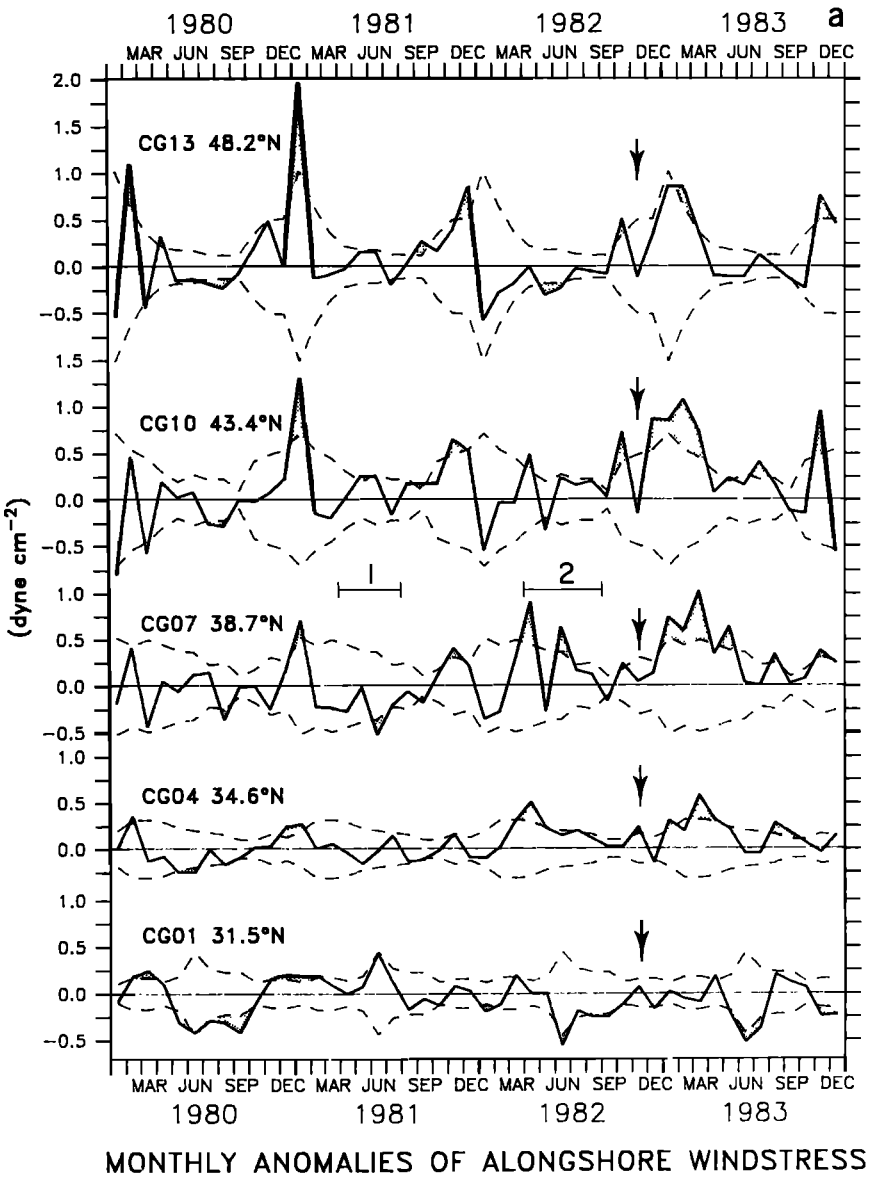

Fig. 17. Anomalies of monthly alongshore calculated wind stress and ASL, 1980–1983. Monthly means of the 6-hourly data were formed for 9 years (Tables 2 and 3). These were used to form the mean and standard deviation for each calendar month and the time series of monthly anomalies from the 9-year average monthly cycle (solid line). The dashed line shows ±1 standard deviation for each calendar month. Shading denotes anomalies greater than 1 standard deviation. The CODE periods are shown by lines labeled 1 and 2, and arrows point to values for November 1982.

value and the average monthly seasonal cycle found from the 9 years of monthly values). The standard deviations of the monthly values for each calendar month (the average anomaly found from the 9 years of monthly values) are also plotted as dashed lines. Monthly anomalies greater than 1 standard deviation have been shaded in.

By comparing the spring and summer periods of 1981 and 1982 (CODE 1 and CODE 2), Figures 15 and 17 show that in 1981, southward winds were stronger than average near 39°N (but greater than 1 standard deviation only during June), ASL values were lower than average everywhere north of 35°N (often by more than 1 standard deviation), currents at 39°N were more southward, and water temperatures were slightly lower. During the spring and summer of 1982, southward winds stress was generally 1 standard deviation or more weaker than normal (except during May) between 35°N and 43°N, sea levels and water temperatures were higher between 37°N and 42°N, and southward currents were weaker at 39°N, except for August. Strong southward winds were experienced in May 1982 at 39°N and to the north, and these resulted in a drop in ASL northward of 42°N and a drop in water temperature northward of 37°N. These winds may have caused the stronger southward currents at 43°N but did not do so at 39°N. The correspondence of monthly wind stress and monthly currents does not appear good, except at the shelf break at 48°N. The fall and winter of 1981–1982 was characterized by strong fall storms at 39°N and to the north, with northward winds greater by 1 standard deviation or more. These winds relaxed in late December, resumed in February, and continued into April, until the transition to southward winds in late April. Temperatures and ASL reflect the wind forcing north of 39°N, with high values in fall, a drop in January, and then either a rise (ASL) or no change (temperature) until May. Currents everywhere

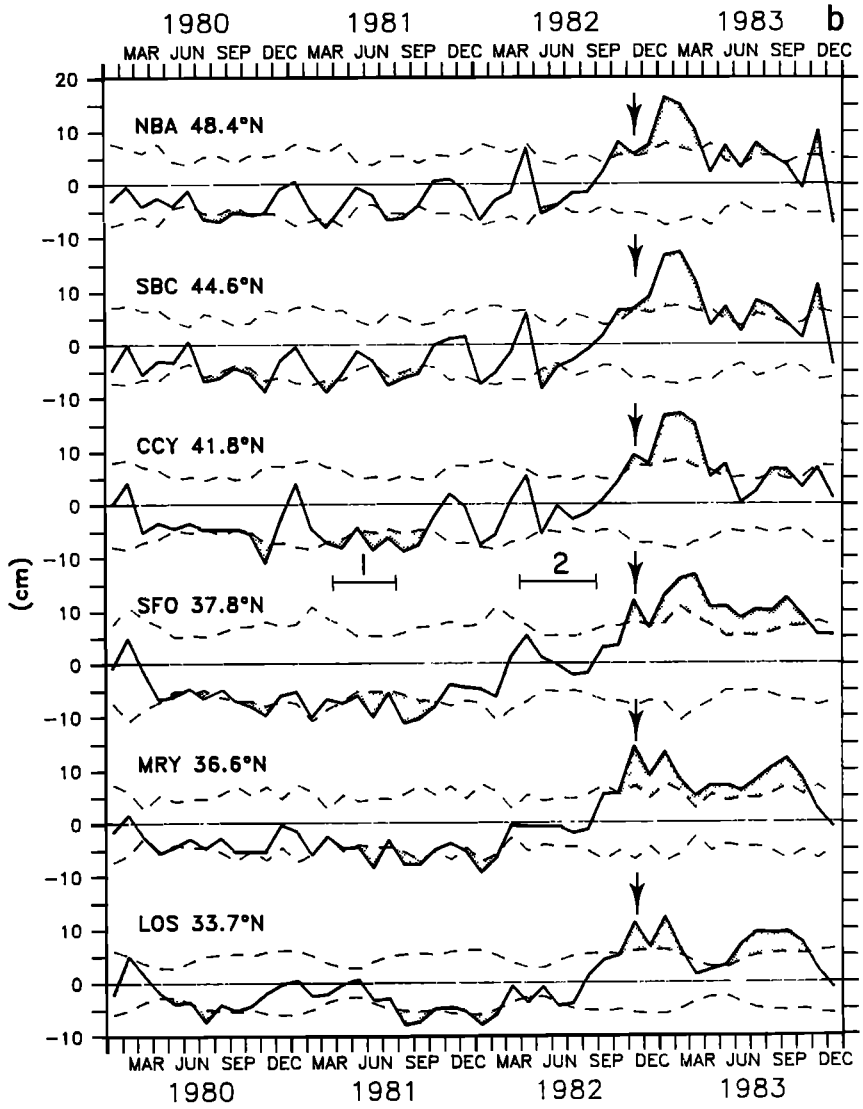

Fig. 17. (continued)

were northward in the fall and were most strongly so at 48°N. After fall, only the 48°N monthly mean currents resemble the local monthly mean wind stress. There is poorest correspondence between monthly wind and currents at 35°N. The wind stress and sea levels around 39°N suggest that the coastal ocean experienced stronger than usual upwelling forcing and response during spring and summer 1981, while the opposite was true in 1982 (with the exception of May 1982 north of 39°N).

In Figure 16 the monthly standard deviations of 6-hourly measured wind stress and ASL show similar patterns, with strong seasonal cycles in the north becoming much less seasonal to the south. The northern seasonal pattern shows much greater short-period variability from fall until mid-spring. The magnitude of the short-period variability in alongshore current is also much greater at 39°N and 43°N than farther north or south, with less seasonality at 39°N. The short-period variability of the temperature signal appears to be dominated by the sharp seasonal transitions in the fall and spring; these produce a large monthly standard deviation that does not represent the magnitude of short-period fluctuations. Further analysis of short-period variability in the wind and current data during the two CODE field seasons is reported by *Denbo and Allen* [this issue] and *Halliwell and Allen* [this issue].

Figures 15, 16, and 17 suggest that the period April 1981 to August 1982 (the SuperCODE period used to estimate the seasonal cycles reported here) was not extraordinary, either in the monthly wind and sea level or in the monthly means of shorter-period variations. Winds were closer to the seasonal cycle during this period than were the high winds of the winters before and after it, and sea levels were more normal than the high sea levels that followed during the 1982–1983 El Niño (Figures 15 and 17).

With regard to the El Niño itself, Figure 15 shows that the strong northward currents and high temperatures that accompany the high sea levels at 43°N during the El Niño are also seen during November 1982 (the last month of data) at 39°N. The temperature and salinity anomalies that accompanied the El Niño off California between 36°N and 38°N have been described in detail by *Rienecker and Mooers* [1986]. Figures 15 and 17 also clearly show that the first peak

of very high sea level in November 1982 between 33°N and 39°N was not accompanied by highly anomalous wind stresses. Though the wind stress at 35°N does show a slightly northward anomaly (approximately 0.25 dyn/cm^2) in Figure 17, it would be hard to argue that this was responsible for the large ASL anomaly seen from 34°N to 48°N. This first peak of anomalous sea level was even more pronounced off central and southern California than it was off Oregon, where it was noted by *Huyer and Smith* [1985].

Conclusions

1. The seasonal cycles of measured wind stress confirm that the magnitude of the seasonal cycle is maximum around 40°N and that annual mean winds change from northward at latitudes north of 40°N to southward at latitudes south of 40°N. At some latitudes south of 38°N a semiannual signal is seen in the seasonal cycles of measured wind stress but not in those of the calculated wind stress. Because of the limited length of the directly measured wind data, the presence of a semiannual signal in alongshore wind stress in the south must be taken as a tentative finding.

2. The picture of alongshore coastal currents derived in earlier studies can be combined with the present data to describe roughly three regimes between 35°N and 48°N. (1) From 45°N to 48°N, north of the maximum seasonal wind stress signal, the seasonal cycles of currents (midshelf at 45°N and shelf break at 48°N) reach their greatest magnitudes. These currents are southward with baroclinic shear in spring and summer and northward and more barotropic in the fall and winter. The observations of *Freeland et al.* [1984] suggest that currents over midshelf at 48°N are weakly northward in summer. The seasonal cycles account for a large proportion (30% to over 50%) of the variance in these currents. The annual mean current in the middle of the water column is southward, opposing the annual mean wind. Superimposed on these regular seasonal cycles are short-period (periods less than 1 month) fluctuations that are weaker in summer and stronger in fall and winter. (2) In a mid-latitude regime, from 39°N to 43°N, where the seasonal cycle of wind stress is greatest, the seasonal cycles of currents are qualitatively similar to those found to the north but are dominated by the shorter-period fluctuations. In this regime the seasonal cycles account for only 10% to 20% of the variances. At 43°N the shorter-period fluctuations decrease in magnitude in the summer, as they do farther north, but at 39°N they are strong during most of the year. This suggests a geographic transition zone between 43°N and 45°N, from a shelf dominated by large, shorter-period fluctuations south of 43°N to one dominated by smoother seasonal cycles at 45°N. The dynamics of this transition remain to be explained. In the middle-latitude regime in summer, strong barotropic fluctuations are superimposed on the mean baroclinically sheared southward flow; in winter, strong baroclinic fluctuations are superimposed on the mean barotropic northward flow. The annual mean currents over midshelf are weakly northward, whereas over the shelf break at 43°N they are weakly southward at 35 m and are northward deeper in the water column. (3) In the south around 35°N the annual mean currents are northward, in opposition to the annual mean wind. The period of sheared, southward currents over the shelf is limited to 1–3 months in spring. During the rest of the year a fluctuating but northward (monthly mean) current exists. The seasonal cycles account for only 10% to 20% of the variances in the alongshore currents, as they do from 39°N to 43°N. The seasonal mean northward current appears (from hydrography) to extend over the slope and may have a semiannual nature, with peaks in early summer and early winter, similar to those found by *Chelton* [1984] in the undercurrent farther offshore at the same latitude. These peaks are roughly coincident with periods of relaxation seen in the measured winds.

3. Temperature and sea level seasonal cycles have the greatest magnitude in the middle latitudes (39°N to 45°N). Both drop suddenly in spring, especially at 39°N, and increase suddenly in fall, especially at 43°N. These transitions decrease in the far north (48°N) and south (35°N), as do the seasonal cycles themselves. Temperatures have less short-period variability, and their seasonal cycles account for 30% to 80% of their variances, while sea level cycles account for 30% to 50% of their variances.

4. The seasonal cycles of alongshore currents lead those of ASL slightly, and both lead those of the wind and temperature by ~1–2 months, confirming results of *Hickey* [1979] and *Chelton* [1984], who lacked simultaneous directly measured currents. An approximate 2-month lag between the summer regime in the south and in the north is seen in all variables. This lag has been documented previously in sea level [*Enfield and Allen,* 1980], calculated wind stress [*Bakun,* 1973, 1975], and climatological wind stress data from ship reports [*Nelson,* 1977].

5. Use of long records of sea level (up to 34 years) and moderately long records of calculated wind stress (9 years) suggests that the overall 1981–1982 period is relatively average. The year prior to the CODE 1 field experiment experienced high winter winds and low short-term variability in sea level. The year following the CODE 2 field experiment experienced stronger winter winds and high sea levels of the 1982–1983 El Niño. The 1981–1982 period is characterized by slightly stronger spring-summer winds and upwelling in 1981, strong fall northward winds and high sea levels, a relaxation of winter winds in the north in January 1982, a late transition from renewed northward winds to southward winds in April 1982, and weaker than usual southward winds (except May) and higher sea levels at 39°N during summer 1982.

Appendix

Significance of the Harmonic Fits

Several methods were used to test the significance of the harmonic fits to the data. One is a modification of the method used by *Beardsley et al.* [1985*b*], which uses a standard *t*-statistic test. In any test it is important to correct for the degree to which the data are serially correlated [*Davis,* 1976]. Beardsley et al. determine an integral time scale from the lagged autocorrelation function of the time series after removal of the annual harmonic and use this integral time scale to find the number of independent data points in the record. The *t*-statistic is formed from the ratio of the regression coefficient to its estimated uncertainty. The square of the estimated uncertainty is found from the sums of squares of the dependent variable divided by $(N - 2)$ times the sums of squares of the independent variable, where N is the number of independent data points. This is discussed by *Allen and Kundu* [1978], except that they calculate

the integral time scale from the original time series. We removed the annual and semiannual harmonics (as in the work by *Beardsley et al.* [1985*b*]) before determining the integral time scale, then estimated the uncertainty in the coefficient using equation (A4) of *Allen and Kundu* [1978]. An alternative method is to average the original data over the integral time scale (using a simple running boxcar mean and decimating the data to one point every integral time scale) and then to use *t*, *F*, or chi-squared tests of significance as if the data were serially uncorrelated. A third method tested, which became the primary method used, is a form of bootstrap test [*Efron*, 1981; *Willmott et al.*, 1985], which is simple, works well with any linear regression, and makes no assumptions about the statistical distribution of the data. In this method, harmonics are first fit to the original time series; the same series is then scrambled randomly in time, and harmonics are fit to the randomized series. The randomization and refitting are repeated a large number of times (200 in our case), and the histogram of the regression coefficients is examined. The significance of the original fit is taken to be the percent of the randomized fits which yield regression coefficients smaller in magnitude than those obtained in the original fit.

For example, in fitting the 6-hourly alongshore current data from the upper midshelf instrument at 35°N to the sin ($2\omega t$) term, the regression coefficient was 2.32 cm/s, there were 2317 data points in the series, and the standard deviation of the residual was 10.9 cm/s. The standard estimate of the error in the coefficient [*Draper and Smith*, 1966, p. 19] is

$$s/[\Sigma(X_i - \bar{X})^2]^{0.5}$$

where s is the standard deviation of the residual, and X are the dependent variables, here sin ($2\omega t$). The test statistic is the coefficient, divided by its standard error. If the 6-hourly values are used as if they are uncorrelated, the test statistic has a value of 7.36, indicating greater than 99.9% significance. If the method of *Beardsley et al.* [1985*b*] is used, the integral time scale is found to be 3.0 days (twelve 6-hour periods), making the number of independent points 194 and changing the test statistic to 2.13. This indicates an approximate 96.5% significance level for over 100 degrees of freedom. If the 6-hourly data are averaged over every 12 points to yield 194 independent values, the coefficient is found to be 2.42 cm/s, the standard deviation of the residual is 9.75 cm/s, and the test statistic is 2.44, indicating a significance level between 98% and 99% ($t(100, 0.98) = 2.32$). If the same 194 points are scrambled and refit 200 times, it is found that only 4 of the 200 random regression coefficients are greater in magnitude than 2.42 cm/s, indicating an approximate 98% significance level.

This example illustrates the difference between the three methods. By using the bootstrap method to indicate the significance level, it was found that the method of *Beardsley et al.* [1985*b*] often produced a test statistic that indicated slightly lower significance than the bootstrap statistic, while the method of averaging over the integral time scale produced a test statistic that often indicated slightly greater significance than the bootstrap method. For marginally significant coefficients this means that a rigorous use of the test statistic at the 95% level would yield different results using the different methods. In the harmonic fits performed here a relatively loose 80% significance cutoff was used with the bootstrap method; the *t*-statistic test with either averaged data or the original series with the correct degrees of freedom would have given similar results. Use of the original 6-hourly values as if uncorrelated, however, would not. It was found that the annual harmonic was nearly always significant at greater than the 99% level. The semiannual harmonic was included in the composite seasonal cycle if it was significant at the 80% level or more. In most instances, if the significance was greater than 80%, it was greater than 95% (there were few marginal cases). It should be emphasized that the significance of the fits and the uncertainties in the coefficients describe only how well the harmonic cycles account for the variance in the short records of data available for analysis.

Limitation to Two Harmonics

By using the much longer records of monthly ASL data, the average monthly cycles (means of each calendar month) were compared to annual cycles found from fits of one to four harmonics. This comparison showed that use of the first two harmonics reduced the root-mean-square differences between the harmonic cycle and the monthly cycle to 1% to 5% of the range in the seasonal cycles. When higher harmonics ($n = 3, 4$) were included in the fits to the long records, the root-mean-square differences were reduced slightly (to 1–2% of the annual range), but the cycles looked essentially the same. When the higher harmonics were included in fits to the same sea level data which had been truncated to correspond to the shorter mooring periods, the resulting cycles developed higher-frequency bumps that were statistically significant but were not present in fits to the longer data set. Thus although some of the higher harmonics fit the moored current and temperature data with statistical significance, this was due to specific features in the shorter records. For this reason we limited the fits to the annual and semiannual harmonics.

Filling of Moored Data

Comparison between fits to the ASL records for the full mooring periods and fits to data which had gaps matching those of the real moorings indicated that large gaps in several of the mooring records significantly changed the phase of the seasonal cycles determined by fits of two harmonics to those records. For this reason, gaps in the moored data were filled before the final fit. Long gaps were filled by regression to data from nearby instruments, usually the adjacent instrument above or below on the same mooring. Shorter gaps of several days or less were filled by standard autoregression techniques. Before filling the current records by regression to adjacent instruments, complex correlations were performed on the low pass–filtered 6-hourly data to determine the angle of maximum correlation between the currents. The largest angle found was 5°, making little change in the components, and the currents were left in their principal axes orientations during the regressions and subsequent filling. Correlation coefficients between vertically adjacent instruments ranged from 0.84 to 0.92 for alongshore currents and from 0.86 to 0.97 for temperatures.

Acknowledgments. This work was supported by the National Science Foundation under grants OCE 8405232, OCE 8014941, OCE 8411613, and OCE 8417769. We would like to thank D. Chelton and T. Dillon for valuable suggestions regarding statistical methods. K. Brink and two anonymous reviewers suggested improvements to an

earlier version of the manuscript. H. Freeland kindly supplied the Canadian current data. H. Pittock, P. Newberger, G. Halliwell, D. Denbo, and C. Alessi helped process the current meter, wind, and sea level data. J. Richter helped prepare the tables.

REFERENCES

Allen, J. S., and P. K. Kundu, On the momentum, vorticity and mass balance on the Oregon Shelf, *J. Phys. Oceanogr., 8,* 13–27, 1978.

Bakun, A., Coastal upwelling indices, west coast of North America, 1946–71, *Tech. Rep. NMFS SSRF-671,* 103 pp., Natl. Oceanic and Atmos. Admin., Seattle, Wash., 1973.

Bakun, A., Daily and weekly upwelling indices, west coast of North America, 1967–1973, *Tech. Rep. NMFS SSRF-693,* 8 pp., Natl. Oceanic and Atmos. Admin., Seattle, Wash., 1975.

Beardsley, R. C., and L. K. Rosenfeld, Introduction to the CODE-1 moored array and large-scale data report, in CODE-1: Moored Array and Large-Scale Data Report, Tech. Rep. 83-23, edited by L. K. Rosenfeld, pp. 1–16, Woods Hole Oceanogr. Inst., Woods Hole, Mass., 1983.

Beardsley, R. C., R. Limeburner, and L. K. Rosenfeld, Introduction to CODE-2 moored array and large-scale data report, in CODE-2: Moored Array and Large-Scale Data Report, Tech. Rep. 85-35, edited by L. Limeburner, pp. 1–21, Woods Hole Oceanogr. Inst., Woods Hole, Mass., 1985*a*.

Beardsley, R. C., D. C. Chapman, K. H. Brink, S. R. Ramp, and R. Schlitz, The Nantucket Shoals Flux Experiment (NSFE79), part I, A basic description of the current and temperature variability, *J. Phys. Oceanogr., 15,* 713–748, 1985*b*.

Chelton, D. B., Seasonal variability of alongshore geostrophic velocity off central California, *J. Geophys. Res., 89,* 3473–3486, 1984.

Chelton, D. B., R. L. Bernstein, A. Bratkovich, and P. M. Kosro, The central California coastal circulation study, *Eos Trans. AGU,* in press, 1986.

Coastal Ocean Dynamics Experiment Group, Coastal ocean dynamics, *Eos Trans. AGU, 64*(36), 538–540, 1983.

Davis, R. E., Predictability of sea surface temperature and sea level pressure anomalies over the North Pacific Ocean, *J. Phys. Oceanogr., 6,* 249–266, 1976.

Denbo, D. W., and J. S. Allen, Large-scale response to atmospheric forcing of shelf currents and coastal sea level off the west coast of North America: May–July, 1981 and 1982, *J. Geophys. Res.,* this issue.

Denbo, D. W., K. Polzin, J. S. Allen, A. Huyer, and R. L. Smith, Current meter observations over the continental shelf off Oregon and northern California, February 1981–January 1984, *Data Rep. 112,* Coll. of Oceanogr., Oreg. State Univ., Corvallis, 1984.

Draper, N. R., and H. Smith, *Applied Regression Analysis,* 407 pp., Wiley-Interscience, New York, 1966.

Efron, B., Nonparametric estimates of standard error: The jackknife, the bootstrap and other methods, *Biometrica, 68,* 589–599, 1981.

Enfield, D. B., and J. S. Allen, On the structure and dynamics of monthly mean sea level anomalies along the Pacific coast of North and South America, *J. Phys. Oceanogr., 10,* 557–578, 1980.

Freeland, H. J., W. R. Crawford, and R. E. Thomson, Currents along the Pacific coast of Canada, *Atmos. Ocean, 22,* 151–172, 1984.

Godfrey, J. S., and K. R. Ridgway, The large-scale environment of the poleward-flowing Leeuwin Current, Western Australia: Longshore steric height gradients, wind stresses and geostrophic flow, *J. Phys. Oceanogr., 15,* 481–495, 1985.

Halliwell, G. R., Jr., and J. S. Allen, CODE-1: Large-scale wind and sea level observations, in CODE-1: Moored Array and Large-Scale Data Report, Tech. Rep. 83-23, edited by L. K. Rosenfeld, pp. 139–185, 1983.

Halliwell, G. R., Jr., and J. S. Allen, Large-scale sea level response to atmospheric forcing along the west coast of North America, summer 1973, *J. Phys. Oceanogr., 14,* 864–886, 1984.

Halliwell, G. R., Jr., and J. S. Allen, The large-scale coastal wind field along the west coast of North America, 1981–1982, *J. Geophys. Res.,* this issue.

Hickey, B. M., The California Current System—Hypotheses and facts, *Progr. Oceanogr., 8,* 191–279, 1979.

Huyer, A., and R. L. Smith, The signature of El Nino off Oregon, 1982–1983, *J. Geophys. Res., 90,* 7133–7142, 1985.

Huyer, A., R. D. Pillsbury, and R. L. Smith, Seasonal variation of the alongshore velocity field over the continental shelf off Oregon, *Limnol. Oceanogr., 20,* 90–95, 1975.

Huyer, A., R. L. Smith, and E. J. Sobey, Seasonal differences in low-frequency current fluctuations over the Oregon continental shelf, *J. Geophys. Res., 83,* 5077–5089, 1978.

Huyer, A., E. J. Sobey, and R. L. Smith, The spring transition in currents over the Oregon continental shelf, *J. Geophys. Res., 84,* 6995–7011, 1979.

Large, W. G., and S. Pond, Open ocean momentum flux measurements in moderate to strong winds, *J. Phys. Oceanogr., 11,* 324–336, 1981.

Lynn, R. J., Seasonal variation of temperature and salinity at 10 m in the California Current, *Rep. 11,* pp. 157–186, Calif. Comm. on Fish., La Jolla, Calif., 1967.

Nelson, C. S., Wind stress and wind stress curl over the California Current, *Rep. NMFS SSRF-714,* 87 pp., Natl. Oceanic and Atmos. Admin., Monterey, Calif., 1977.

Reid, J. L., and A. W. Mantyla, The effect of the geostrophic flow upon coastal sea elevations in the northern North Pacific Ocean, *J. Geophys. Res., 81,* 3100–3110, 1976.

Rienecker, M. M., and C. N. K. Mooers, The 1982–1983 El Nino signal off northern California, *J. Geophys. Res., 91,* 6597–6608, 1986.

Strub, P. T., J. S. Allen, A. Huyer, and R. L. Smith, Large-scale structure of the spring transition in the coastal ocean off western North America, *J. Geophys. Res.,* this issue.

Thomson, R. E., W. R. Crawford, H. J. Freeland, and W. S. Huggett, Low-pass filtered current meter records for the west coast of Vancouver Island: Coastal Oceanic Dynamics Experiment, 1979–81, *Data Rep. Hydrogr. Ocean Sci. 40,* 102 pp., Instit. of Ocean Sci., Sidney, British Columbia, Canada, 1985.

Wickham, J. B., A. A. Bird, and C. N. K. Mooers, Mean and variable flow over the central California continental margin, 1978 to 1980, *Continental Shelf Res.,* in press, 1986.

Willmott, C. J., S. G. Ackleson, R. E. Davis, J. J. Feddema, K. M. Klink, D. R. Legates, J. O'Donnell, and C. M. Rowe, Statistics for the evaluation and comparison of models, *J. Geophys. Res., 90,* 8995–9005, 1985.

J. S. Allen, A. Huyer, R. L. Smith, and P. T. Strub, College of Oceanography, Oregon State University, Corvallis, OR 97330.

R. C. Beardsley, Woods Hole Oceanographic Institution, Woods Hole, MA 02543.

(Received March 10, 1986;
accepted May 27, 1986.)